Eindhoven University of Technology

MASTER

A molecular dynamics study of the Gibbs elasticity of interfaces

van Noije, T.P.C.

Award date:
1995

Eindhoven University of Technology
Department of Applied Physics
Theoretical Physics

A Molecular Dynamics study
of the Gibbs elasticity
# of interfaces

Twan P.C. van Noije

Preface

First of all I would like to thank Guy Verbist for his trust and advise. He has given me plenty of opportunities to get acquainted with the field of computer simulation in chemical physics. Thanks Guy !

Two other persons I would like to thank for introducing me to this field, are Sami Karaborni and Berend Smit.

Further, I wish to thank Thijs Michels and Guy for their help in finding a Ph.D. position.

Thanks to all members of the Engineering Physics department, including Trijntje and Astrid, all trainees that I have met in the course of the year and everybody else, I have had a great time in Amsterdam.

Abstract

In this thesis a study of the stability of liquid films and foams is performed. The stability of films and interfaces is governed by their elastic properties. In equilibrium, these elastic properties are quantified by the Gibbs elasticity, expressing the dependence of the surface tension on an extension or contraction of the interface(s). Our main interest is to study this dependence as a function of the presence of surface-active molecules (surfactants).

The Gibbs elasticity of interfaces is studied by simulation. To this end a Molecular Dynamics program has been developed. In the simulations, a simple generic model of interfaces is used. The model interactions determine the subsequent configurations of the particles at the interface. Thermodynamic properties of the interface are averages over these configurations.

In contrast to the surface tension, the Gibbs elasticity is a fluctuation. Fluctuations are far more difficult to obtain from a simulation than simple linear averages. Furthermore, the thermodynamics of fluctuations is a topic that is not fully discussed in literature.

This thesis has been organized as follows. Chapter 1 illustrates the relation between the stability of films and foams and the Gibbs elasticity. General aspects of simulation in classical statistical mechanics are discussed in chapter 2. In chapter 3 the Molecular Dynamics method is explained. Techniques to obtain a constant temperature are emphasized, since the calculated Gibbs elasticity is expected to be strongly dependent on their quality. In chapter 4, fluctuation formulae are derived for thermodynamic quantities, in particular for the Gibbs elasticity. Chapter 5 discusses methods to estimate errors in quantities calculated by simulation. It is shown that estimating errors in fluctuations is not trivial. Molecular Dynamics simulations of bulk systems consisting of Lennard-Jones particles, are described in chapter 6. The reason is that the interfaces are modelled as two repulsive liquids, each of which consists of Lennard-Jones particles. This is explained in chapter 7. Here, results are presented for the dependence of the surface tension and the Gibbs elasticity on the concentration of surface-active molecules present at the interfaces. The calculation of the Gibbs elasticity is a time-consuming activity, if one realizes that a simple calculation (at a given concentration) takes approximately 2 days on the IBM Scalable Power 2.

Contents

Chapter 1

Introduction

1.1 Surface tension and elasticity

Atoms or molecules in boundary regions have a different environment than those in bulk regions. For a liquid-vapour surface, this is a result of the particle density difference across the surface. Particles in the liquid phase near the surface do not have as many neighbours as those in the bulk liquid. Since the interactions of interest are attractive[1], in many cases van der Waals forces, particles near the surface experience an attraction into the liquid. This results in a tendency of the surface to minimize its area. This tendency can be expressed in a surface tension, which is the force in the surface acting on a line of unit length drawn in the surface. We will always assume that this tension is uniform, i.e. it is perpendicular to any line drawn in the surface and its magnitude is independent of the direction of this line and the position on the surface. For systems in equilibrium at a constant temperature T, the surface tension γ can be defined as the derivative of the free energy F with respect to the interfacial area A,

$$\gamma = \frac{\partial F}{\partial A}, \tag{1.1}$$

where the other independent macroscopic variables, as temperature, are kept constant. Since systems in equilibrium at a constant temperature have a minimal free energy, a positive surface tension expresses a tendency to minimize the interfacial area.

An interface between two immiscible liquids shows the same tendency, which in this case is the result of repulsive interactions across the interface. We will use the name surface tension for the liquid-vapour surface as well as the liquid-liquid interface, although strictly speaking it should be interface tension in the latter case.

Provided that there is a difference of polarity across the interface, as in the case of liquid-vapour surfaces of polar fluids and liquid-liquid interfaces as the oil-water interface, surface tensions can be affected by the addition of amphipathic molecules. These molecules consist of a spatially separated hydrophilic and hydrophobic part. The hydrophilic part, which is called the head of the molecule, is attracted to polar phases, whereas the hydrophobic tail prefers apolar phases. Addition of these molecules results in a stronger attraction across the interface, i.e. in a decrease of surface tension. Making the demand of minimal interfacial area less severe, these so-called surfactant molecules increase the foaming ability of a liquid-gas interface or the mixing ability of two immiscible liquid phases, respectively.

The stability of an interface is largely determined by the dependence of the surface tension on the presence of amphipathic molecules. If an interface is perturbed from equilibrium in such a way that locally its area is increased, the local area density of amphipathic molecules will

---

[1]Attractive forces are essential for the liquid-vapour coexistence; particles with only repulsive interactions do not show a liquid-vapour transition.
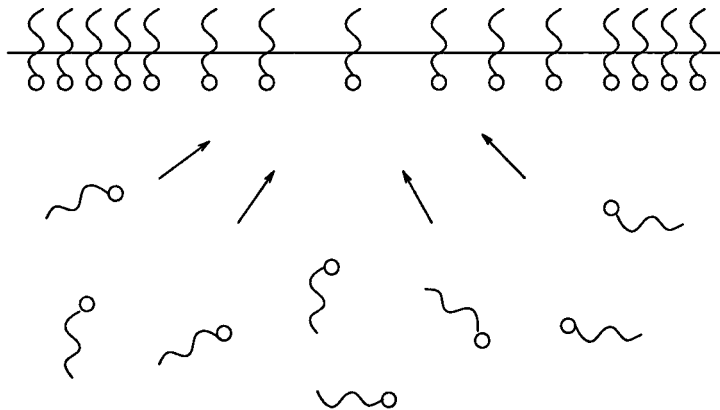
Figure 1.1: *A locally expanded surface tends to contract due to the locally increased surface tension. Diffusion from the bulk counteracts this stabilizing effect.*

decrease. As a consequence the surface tension will increase locally. The locally increased force will restore the interface to its equilibrium configuration. This stabilizing effect is known as the Marangoni effect. The Marangoni effect is a dynamic effect in the sense, that a low area concentration of amphipathic molecules induces diffusion from the bulk phase to the interface (see figure 1.1). Time scales involved in these processes are of importance to the stability of interfaces.

Since the Marangoni effect is a result of the dependence of the surface tension on the area density of amphipathic molecules, it is closely related to the dependence of the surface tension on the interfacial area. This dependence is expressed by the surface elasticity, which was first introduced by Gibbs [1] as

$$\varepsilon = \frac{\partial \gamma}{\partial \ln A},\qquad(1.2)$$

again at constant temperature.

The difference, however, is that the Gibbs elasticity is defined under equilibrium conditions, whereas the Marangoni effect is a dynamic effect. Therefore, no simple relationship between the Marangoni effect and the Gibbs elasticity has been found. In this thesis we will be studying systems in equilibrium. For these systems, stability criteria for interfaces can be expressed in terms of the Gibbs elasticity.

In the next section we will discuss some experimental studies on the elasticity of films and surfaces. In section 1.3 and 1.4 we will illustrate the role of the elasticity in the stability of films and foams, respectively.

1.2 Experimental studies on elasticity

In this section we want to give an impression of some experimental studies on elasticities of films and surfaces. We will start with a description of a technique published by Prins et al. in 1967 [2].

The elasticity of films of thicknesses of the order of 10^{-4} cm was measured. Films of these thicknesses will be referred to as thick films. The elasticity of a film is defined as

$$\frac{2d\gamma}{d\ln A},\tag{1.3}$$

where the factor 2 arises because the film has two surfaces (A is the area of the film).

Liquid films were formed between the thin wires of two vertical frames, after immersion in a surfactant solution. The frames were moved vertically in such a way that one frame moves up while the other goes down. In this way the total surface area of the surfactant solution did not change. During the upward movement of one frame, new film is drawn from the solution. This new film, much thicker than the lower part of the original film, acted as a load for the original film. Due to this load the original film was extended. The change in area of an element in the original film was related to the change in its thickness. This decrease in thickness was measured from the displacement of the interference fringes (corrected for the contribution of drainage).

The corresponding change in surface tension was found by assuming mechanical equilibrium. Then the weight of the film is supported completely by a vertical gradient in the surface tension. This will be explained in the next section. The procedure consisted of measuring the total weight of the film present between the film element considered and the horizontal solution surface.

The film elasticity was obtained as a function of film thickness for relatively high concentrations (see figure 1.2). For this concentration regime, the film elasticity was found to decrease with increasing film thickness due to diffusional interchange of surfactants between the surfaces and the solution in the film. Since in thicker films there are more surfactants in solution near the surfaces, the diffusional effect is larger in thicker films.

There is a concentration above which surfactants in solution form complexes called micelles. The corresponding concentration is the critical micellar concentration (c.m.c.). In a micelle, the surfactants point their hydrophilic head towards the water phase, while their hydrophobic tails form the interior of the micelle, which is depleted of water. Due to the formation of micelles, the surface concentration does not increase with increasing bulk concentration above the c.m.c. Therefore, the surface tension shows a plateau above the c.m.c. (see figure 1.3). Above the c.m.c., Prins et al. found the film elasticity to be an order smaller than below the c.m.c. due to an increased diffusional effect (the micelles forming an extra reservoir). Also above the c.m.c. the film elasticity decreased with film thickness.

Another method to measure elasticity was published in 1975 by Lucassen and Giles [3]. Here it concerned measurements of the elasticity of a surface[2]. Surfaces of surfactant solutions were subjected to area variations in the form of small harmonic longitudinal waves. This compression and expansion of the surface was performed at a constant temperature. Surface tension variations resulting from the area variations were measured by the Wilhelmy plate method. In this method, the force acting on a small vertical plate touching the surface exactly, is measured by a microbalance.

For insoluble monolayers, where there is no diffusional interchange of surfactants between the surface and the solution, the surface tension followed the area changes instantaneously. For higher concentrations, a non-zero phase angle θ was observed. Then the surface elasticity was written as $\varepsilon = |\varepsilon| \exp{(i\theta)}$. The absolute value $|\varepsilon|$ was obtained within an error of 1% as a function of both concentration of the solution and frequency of the longitudinal waves (see figure 1.4).

The absolute value of the surface elasticity was found to increase with the bulk concentration of the solution for low concentrations. This concentration regime will be referred to as the

---

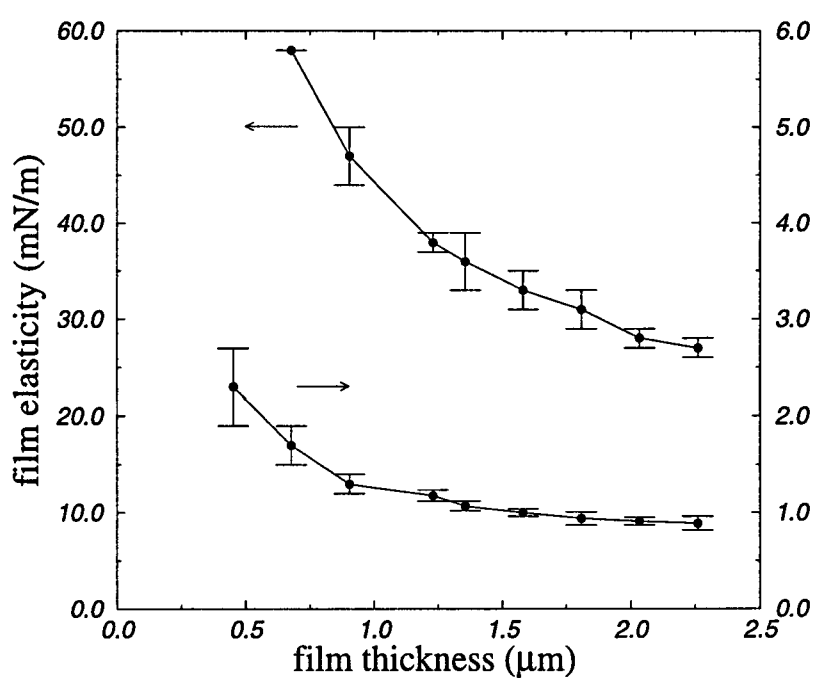[2]Some authors refer to surface elasticity as surface dilational modulus and to film elasticity as Gibbs elasticity.

Figure 1.2: *Film elasticity as a function of film thickness as found by Prins et al. The upper curve corresponds to a bulk concentration $4\,10^{-6}$ mol/cm^3 and the lower curve to $15\,10^{-6}$ mol/cm^3, which is above the c.m.c. $5\,10^{-6}$ mol/cm^3. Films drawn from solutions of sodium dodecyl sulfate (SDS).*
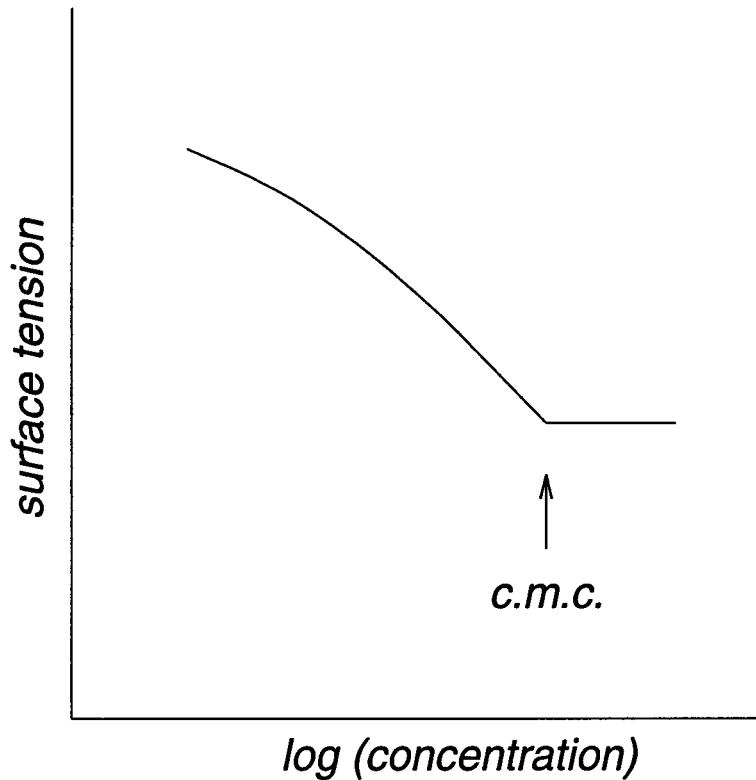
Figure 1.3: *A sketch of the dependence of the surface tension on the bulk concentration.*

insoluble monolayer regime, since diffusional effects are small. For larger concentrations $|\varepsilon|$ decreased with increasing bulk concentration, due to a dominating diffusional effect. The maximum in the surface elasticity was found for concentrations below the c.m.c. Above the c.m.c. additional diffusion mechanisms caused the surface tension to decrease more quickly with increasing concentration.

The absolute value of the surface elasticity showed no frequency dependence in the low concentration limit. For higher concentrations the surface elasticity was found to increase with increasing frequency. The frequency dependence, growing with increasing concentration, could be explained from the dynamics of the diffusion processes. The region from which surfactants can reach the surface in the time of expansion of the surface, is smaller at higher frequencies than at lower frequencies. It was shown that this frequency dependence can be mapped on the dependence of the film elasticity on film thickness, if for the film thickness is chosen

$$h = 2\sqrt{\frac{D}{\omega}}, \tag{1.4}$$

where D is the diffusion coefficient of the surfactants and ω the angular frequency. Using this relation, film elasticities at a given thickness and surface elasticities at the corresponding frequency can be compared (see figure 1.5). For low as well as high concentrations, the film elasticity is simply twice the surface elasticity. For intermediate concentrations (around the elasticity maximum), the deviation is very small.
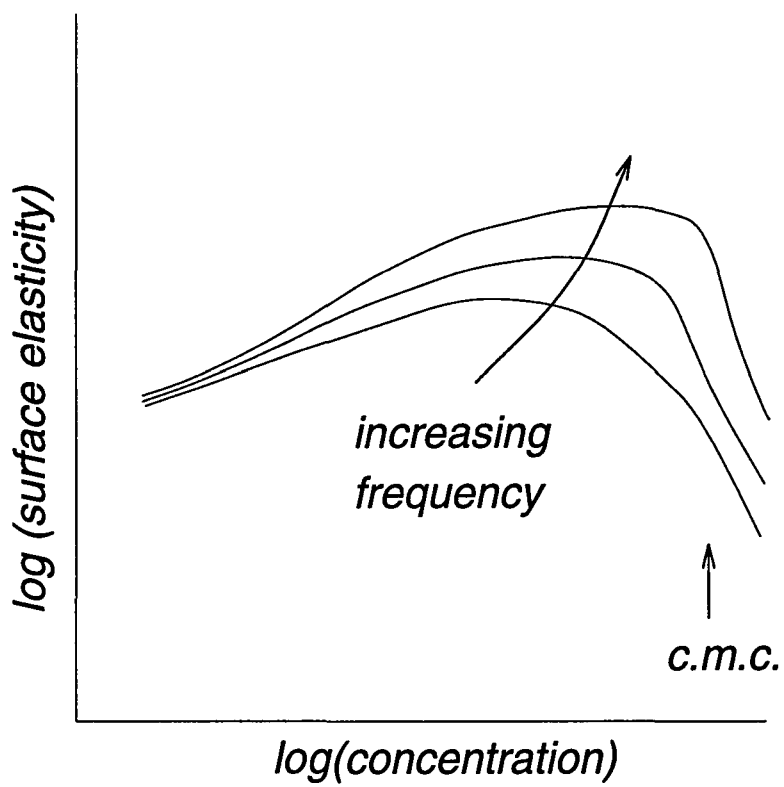
Figure 1.4: *Sketch of the absolute value of the surface elasticity* $|\varepsilon|$ *as a function of bulk concentration at different frequencies.*
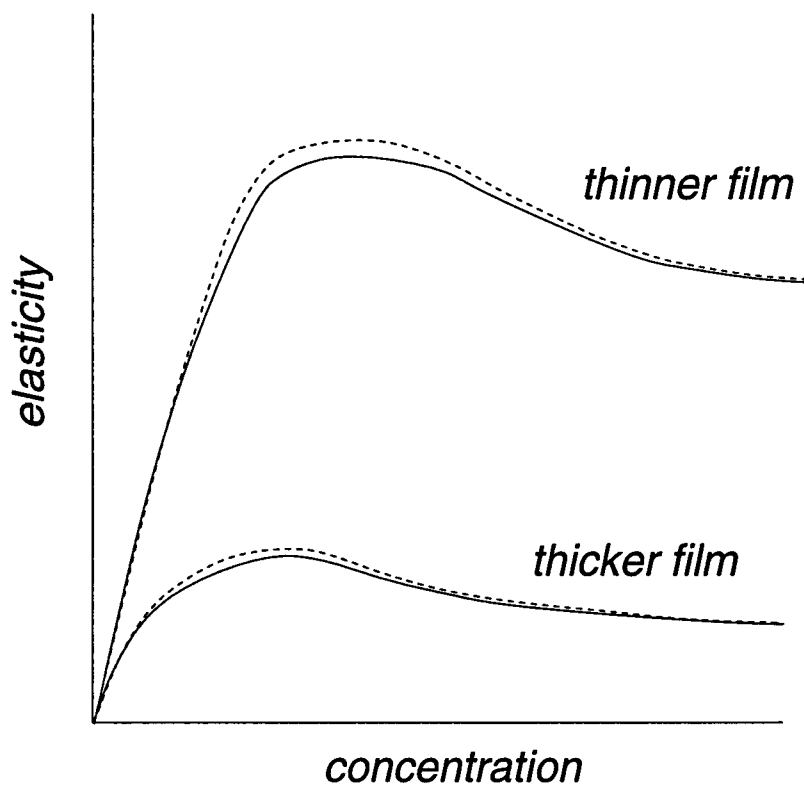
Figure 1.5: *Elasticity as a function of bulk concentration. Solid curves represent half the film elasticity at a certain thickness, whereas dashed curves represent the surface elasticity at the corresponding frequency. The two upper curves correspond to a thinner film (or higher frequency).*
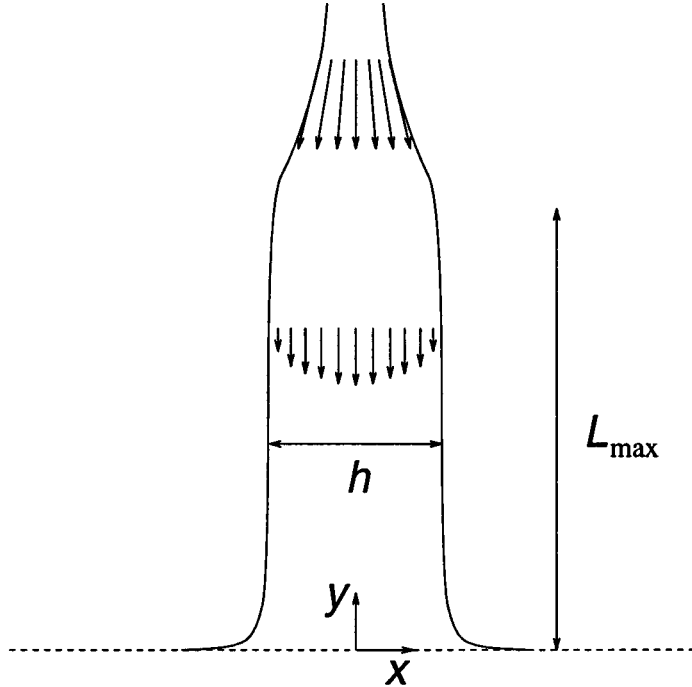
Figure 1.6: *The effect of insoluble monolayers on the flow in a vertical free film.*

1.3 Film stability

Two stages in the history of a film are critical to rupture. The first is just after its birth when the film is young and thick, the other is much later when it is old and thin after drainage. Rupture of thin films (of thicknesses below a few hundred nanometers) is a consequence of the interaction between the two approaching surfaces of the film. These interactions involve electrostatic repulsion, van der Waals attraction and steric repulsion. In general a thin film will be instable if a thickness fluctuation will grow. For an attractive interaction this is the case if the attraction increases with decreasing thickness.

Rupture of thick films is determined by their dynamic elastic properties. This will be illustrated below for the case of a vertical film in a gravitational field. For a general review on the dynamic properties of free liquid films and foams, we refer to Lucassen [4].

Consider a vertical, free liquid film with surfaces covered with an insoluble monolayer (see figure 1.6). The downward velocity $-v_y$ is governed by the Navier-Stokes equation for Stokes flow (stationary, incompressible flow of low Reynolds number)

$$\eta \frac{d^2 v_y}{dx^2} = \rho g, \tag{1.5}$$

where η is the viscosity of the liquid, ρ its mass density and g the gravitational acceleration. The presence of the monolayer forces the velocity at the boundaries to be zero in the lower part of the film , i.e. $v_y (\pm h/2) = 0$, yielding the parabolic velocity profile

$$v_y = -\frac{\rho g}{2\eta} \left(\left(\frac{h}{2} \right)^2 - x^2 \right). \tag{1.6}$$

This is only possible if the stress exerted by the flowing liquid is balanced by a surface tension gradient

$$\frac{d\gamma}{dy} = \eta \left. \frac{dv_y}{dx}\right|_{\frac{1}{2}h} = \frac{\rho g h}{2}. \tag{1.7}$$

Although flow is essential in creating a surface tension gradient, this relation also applies for very high viscosities, where the rate of flow is negligibly small. In that case it is more obvious that the weight of film elements should be balanced by a tension difference.

Since the tension difference is bounded to a maximum (namely the tension of the pure liquid minus the minimal tension that can be reached for the monolayer in question), there is a maximal height where the tension can just support the weight of the film below. From equation 1.7 this maximum height is inversely proportional to the film thickness as

$$L_{\max} = \frac{2\Delta\gamma}{\rho g h} \tag{1.8}$$

For aqueous films the maximum surface tension difference $\Delta\gamma$ is of the order of 50 mN/m, leading to

$$L_{\max} = \frac{1}{10h}, \tag{1.9}$$

with lengths expressed in cm. Above this maximal length a surface tension gradient is absent. Therefore the viscous stress should vanish at both surfaces and as a result there will be no velocity gradient in the x-direction (plug flow). Film elements will simply and quickly be extended. Since the rate of extension is increasing with height, the film as a whole will undergo a catastrophic rupture process. This process is initiated at high thicknesses (equation 1.8).

So far we have considered the case where the film is covered with insoluble monolayers. In this regime the film elasticity, at a given low surfactant concentration, is independent of thickness. An extension of a film element then leads to a decrease in film elasticity of this element, because of surfactant depletion. Thinner parts of the film thus have a lower resistance to thinning than thicker parts. Therefore, insoluble monolayers are usually unsuitable as film stabilizers (although the film elasticity can be quite large).

On the other hand, films in which the thickness dependence is dominated by diffusional exchange with the film liquid, i.e. at higher surfactant concentration where the film elasticity decreases with increasing liquid concentration, show a stabilizing effect. During extension the liquid concentration in these films decreases, which means that the film elasticity increases with decreasing film thickness.

When the adsorption isotherm, relating the surface and bulk concentrations, is known, the shape of a film just after its formation can be calculated. A qualitative impression is given in figure 1.7. On the left is shown a film in the insoluble regime. The film elasticity is lower in the thinner parts of the film. On the right a film at a higher concentration is shown. Due to diffusion the film elasticity shows an opposite dependence on film thickness.

1.4 Foam stability

In a foam, individual films are separated from each other by liquid channels, the Plateau borders (see figure 1.8). The interplay between a Plateau border and the films is a crucial factor in foam generation and stability. To illustrate this, consider a foam which is subjected to deformation. The foam films will tend to either increase or decrease in area. However, they can never do so in isolation and the Plateau borders will have to be involved in the deformation too. To first approximation, the tension should be uniform during the joint deformation. As a consequence, the ratio between the relative extensions of the Plateau border and the film is inversely proportional to the ratio between their elasticities. Since for most surfactant solutions, the elasticity of the Plateau border is much smaller than that of the adjoining film (due to diffusion of surfactants),
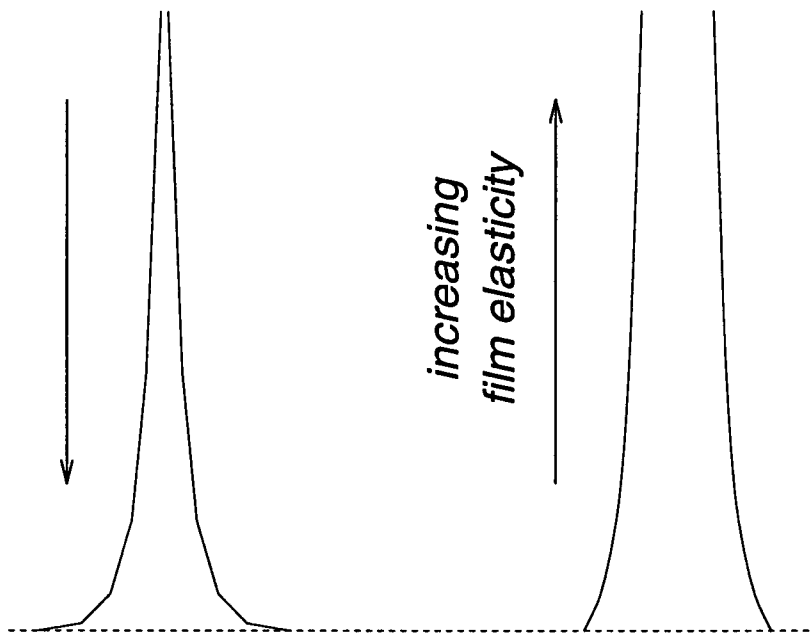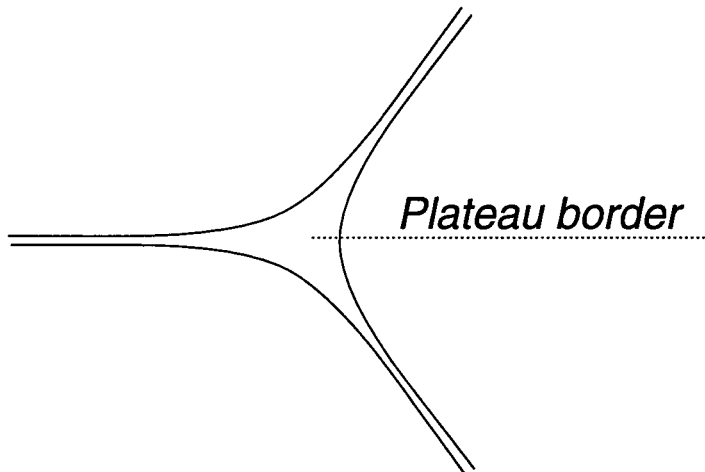
Figure 1.7: *Film profiles just after formation. The film on the left is in the insoluble regime, whereas the film on the right in the diffusion dominated regime. The film elasticity increases along the arrows.*

Figure 1.8: *The junction of three foam films.*

the extension of the Plateau border is much larger. The result is that new thick film is being pulled out of the Plateau border. The Plateau borders then act as a buffer against deformation, in such a way that the films are protected against rupture.

The interaction between foam films and Plateau borders involve more processes than the one described above. Under certain circumstances, the Plateau borders can have an accelerating effect on the thinning of the films, called marginal regeneration. For a discussion of this effect, we refer to Lucassen [4]. Another effect that can cause foams to disappear is bubble disproportionation, due to diffusion of gas from smaller bubbles to larger ones. The foam can then collapse without any of its films actually breaking. In two dimensions (no gravity) this effect has been described by Weaire and Rivier [5] and Glazier and Weaire [6]. In three dimensions drainage of the foam due to gravity (described by Verbist and Weaire [7]) causes rupture of films to dominate bubble disproportionation. Below, we will discuss the stability of spheres embedded in a larger medium. These spheres can either be drops or bubbles.

For a general curved interface we have to consider the pressure difference across the interface, which in equilibrium is related to the surface tension by the Laplace-Young equation

$$\Delta p = \gamma \left(\frac{1}{R_1} + \frac{1}{R_2} \right). \tag{1.10}$$

The principal radii of curvature R_1 and R_2 are locally defined as the maximum and minimum radii of curvature of the interface. If the pressure difference equals zero, the Laplace-Young equation reduces to $1/R_1 + 1/R_2 = 0$, which is the condition of minimal area for interfaces that are closed or have a fixed boundary. In order to derive stability criteria, we will focus on two simple cases, both involving spherical interfaces.

First we will consider a spherical region of a particular phase at a pressure p entirely surrounded by an indefinitely large region of·a different phase at a pressure p_0. In this case the free

energy is a function of the sphere volume and area $F(V(r), A(r))$. The equilibrium condition $\partial F/\partial r = 0$ can be written out as

$$\frac{\partial F}{\partial r} = \frac{\partial F}{\partial V}\frac{\partial V}{\partial r} + \frac{\partial F}{\partial A}\frac{\partial A}{\partial r} = -(p - p_0)4\pi r^2 + \gamma 8\pi r = 0, \tag{1.11}$$

which directly yields the Laplace-Young equation for spherical interfaces

$$\Delta p = \frac{2\gamma}{R}. \tag{1.12}$$

The stability condition $\partial^2 F/\partial r^2 > 0$, or more explicitly

$$\frac{\partial^2 F}{\partial r^2} = -\frac{\partial p}{\partial r}4\pi r^2 - \Delta p 8\pi r + \frac{\partial \gamma}{\partial A}(8\pi r)^2 + \gamma 8\pi > 0, \tag{1.13}$$

reduces to

$$\varepsilon - \frac{\gamma}{2} > \frac{R^2}{4}\left.\frac{\partial p}{\partial r}\right|_R. \tag{1.14}$$

Here the pressure dependence on volume appears as a stabilizing effect.

Next consider the equilibrium of two spheres of a particular phase at the same pressure, embedded in another phase. Equal pressures can be established by connecting the spheres by a thin pipe. In equilibrium the radii of the spheres are equal. In order for the two spheres to be in stable equilibrium, a small transfer of particles from sphere 1 to sphere 2, giving rise to an increase in the radius of sphere 2, should be followed by a pressure increase in sphere 2. This stability condition that for both spheres $\partial p/\partial r$ should be positive, reduces to

$$\varepsilon - \frac{\gamma}{2} > 0, \tag{1.15}$$

which only involves the surface tension and elasticity. Equation 1.15 is also applicable to a system of two equal-sized bubbles in a foam. In this case the surface tension and the Gibbs elasticity refer to both surfaces constituting the film of the bubbles.

Chapter 2

Classical statistical mechanics

2.1 The classical approximation

We are interested in macroscopic properties of many-particle systems. At a microscopic level the time evolution of the system can be described by either quantum or classical mechanics. We will be considering classical systems only.

For atomic systems the classical approximation holds, if the de Broglie thermal wavelength, defined as

$$\Lambda = \left(\frac{2\pi\hbar^2}{k_B T m} \right)^{1/2},$$ (2.1)

is much smaller than the mean nearest-neighbour separation, which can be approximated by $\rho^{-1/3}$ with ρ the number density. ($\hbar$ is the Planck constant divided by 2π, k_B the Boltzmann constant and m the atomic mass.) For molecular systems, there are additional requirements for the rotational and vibrational degrees of freedom. The classical approximation leads to important simplifications, because kinetic and potential contributions to thermodynamic properties can be separated. Comparision between the total kinetic energy K and total potential energy U, offers a simple means of characterizing the system. For the dilute gas $K/|U| \gg 1$, whereas for the low-temperature solid $K/|U| \ll 1$. For the liquid state K and $|U|$ are comparable. Alternatively, characterizing the interactions in the system by a length σ and energy ϵ, the reduced density $\rho^* = \rho\sigma^3$ and the reduced temperature $T^* = k_B T/\epsilon$ are both of order unity in the liquid state. For a general review on the theory of classical liquids, we refer to Hansen and McDonald [8].

2.2 Ensemble averages

In classical mechanics the state of one particle is described by its position $\underline{r}$ and momentum $\underline{p}$. As a consequence a microscopic state of a classical many-particle system is characterized by the positions and momenta of all particles.

A macroscopic state of a system is characterized by the density of microscopic states in phase space. This density $\rho\left(\underline{r}^N, \underline{p}^N\right)$ expresses the probabilities of all microscopic states the system can be in. (The superscript N refers to the complete particle set.) It is referred to as the ensemble of the macroscopic state. A macroscopic quantity B is defined as the average over the ensemble of the corresponding microscopic quantity $\mathcal{B}\left(\underline{r}^N, \underline{p}^N\right)$ by

$$B = \langle \mathcal{B} \rangle = \frac{\int d\underline{r}^N d\underline{p}^N \mathcal{B} \rho}{\int d\underline{r}^N d\underline{p}^N \rho}.$$ (2.2)

The denominator is the central property of the macroscopic system, since it is proportional to the partition function of the system. From this partition function all thermodynamic properties can be derived.

A system is said to be in equilibrium if its macroscopic state does not change in time. This means that the system can be described by a unique ensemble, corresponding to a time-independent density of microscopic states. For a one-component atomic system some commonly used ensembles are the microcanonical NVE, the canonical NVT, the isothermal-isobaric NpT and the grand canonical μVT ensemble. We will discuss some of these ensembles below.

For instance in the microcanonical ensemble, all microscopic states of the ensemble have the same number of particles N, volume V and energy E. Since N is a constant, we are dealing with a phase space of fixed dimension $6N$ ($3N$ in coordinate space and $3N$ in momentum space). All microscopic states lie on a surface of constant energy E in this space. The position and shape of this surface can be expressed as a function of the volume V only. Since all microscopic states with energy E are equally probable, for the microcanonical ensemble the density of microscopic states is proportional to the Dirac δ-function $\delta(E - \mathcal{H})$, where the Hamiltonian $\mathcal{H}$ depends on atomic positions and momenta.

In the canonical ensemble microscopic states with different energies have different probabilities. The density of microscopic states is proportional to the Boltzmann factor $\exp(-\beta\mathcal{H})$ with $\beta = 1/(k_B T)$. Note that the temperature is constant only in a macroscopic sense. The kinetic energy of the microscopic states of the canonical ensemble does fluctuate for a finite system. As a consequence the instantaneous temperature, which can be defined in terms of this instantaneous kinetic energy, is not constant.

2.3 Ensemble dependence of fluctuations

Macroscopic quantities that can be written as simple *averages* over microscopic states, i.e. $B = \langle B \rangle$, do not depend on the choice of ensemble in the thermodynamic limit of infinite system size. In fact this is only true if the quantity belongs to a certain class of functions. We will always consider quantities that belong to this class and will not go into detail about the necessary subtle criteria (see [9]). For a finite system relative differences are of the order $1/N$.

On the other hand *fluctuations* are ensemble dependent, even for infinite systems. Fluctuations can be expressed as variances or covariances of microscopic quantities. These will be denoted by $\langle (\delta B)^2 \rangle$ and $\langle \delta A \, \delta B \rangle$ respectively, where δB means $B - \langle B \rangle$.[1] Fluctuations show up in thermodynamic derivatives. In this study they play a major role, since we are interested in volume and area dependences of macroscopic quantities, in particular the Gibbs elasticity.

Lebowitz, Percus and Verlet [9] derived expressions to transform fluctuations between ensembles. In the canonical ensemble, fluctuation formulae for derivatives can be found in a straightforward way. In chapter 4, we will derive expressions involving volume and area derivatives in the canonical as well as the microcanonical ensemble. Direct derivation of fluctuations in the microcanonical ensemble is not straightforward. The main reason is the appearance of the Dirac δ-function. Ray and Craben [10] first succeeded in directly deriving expressions for fluctuations in the NVE ensemble. A different approach was followed by Pearson et al. [11], where Laplace transform techniques were applied to deal with the mathematics. We will discuss this approach in chapter 4. Both direct derivations yield expressions consistent with the Lebowitz transformation rules.

---

[1]From the context it will always be clear whether δ refers to the Dirac δ-function or to a deviation from an average value.

2.4   Simulation techniques

We will only consider microscopic quantities that are a function of either the atomic positions or momenta. In the latter case the macroscopic quantity in the canonical ensemble is easily obtained, since the Hamiltonian is a simple quadratic function of the atomic momenta. If the microscopic quantity is a function of atomic positions only, we are still dealing with a non-trivial average over configurational space. For a system interacting through pair potentials only, theory on the system can be developed by approximating this average by diagrammatic cluster expansions.

Another way to attack the problem is by simulation. In 1953 Metropolis, Rosenbluth, Rosenbluth, Teller and Teller [12] introduced a method to sample configurational space in the canonical ensemble. Pioneer work had been done by Mayer, Ulam and Von Neumann. This method is well known as the Monte Carlo (MC) method. The name is due to the random character of the particle moves. Originally, a new microscopic state is generated from the previous one by randomly changing the coordinate of one particle. In order to simulate the canonical ensemble, the following acceptance criterium is used: accept the new state if the energy difference $\Delta\mathcal{H}$ with the old state is negative; if the energy has increased, the new state is accepted with a probability $\exp\left(-\beta\Delta\mathcal{H}\right)$. Since its introduction the Monte Carlo method has been modified in order to make the sampling more efficient. The original method allows the movement of one particle at a time. The freedom in particle moves is bigger than this: each combination of moves is allowed as long as the transition probabilities satisfy the principle of detailed balance.

The Monte Carlo technique can be easily adapted to sample the isothermal-isobaric or grand canonical ensemble. In these ensembles particle moves are combined with volume changes in the NpT ensemble and particle destructions and insertions in the μVT ensemble. Of course the acceptance criteria should be appropriately modified.

Another modified version is the Gibbs ensemble method introduced by Panagiotopoulos [13] to simulate phase equilibria, specifically liquid-vapour coexistence. Up to now it is impossible to simulate 10^{23} particles, instead simulation systems contain 100 to 10^5 particles. Studying phase equilibria in such small systems, the interfacial region dominates the bulk regions. If one is not interested in interfacial properties, the Gibbs ensemble method provides an outcome. Instead of simulating coexistence in one simulation box, the Gibbs ensemble method simulates the liquid and gas bulk phases in two different boxes at the same pressure and chemical potential. Of course interfacial properties cannot be obtained in this way. Starting from the same particle density in both boxes, a combination of particle moves, volume changes and particle exchanges between the boxes leads to phase separation. In equilibrium the boxes of lower and higher concentration correspond to the vapour and liquid phase respectively.

The Monte Carlo method does not give information on the dynamics of the system in question. If one is interested in dynamic behaviour, one can resort to another simulation method, known as Molecular Dynamics (MD). This method will be described in the next chapter. Since the properties of interfaces are affected by processes involving diffusion of surfactants, we have chosen the Molecular Dynamics method. In this thesis, we studied equilibrium properties as the equilibrium surface tension and Gibbs elasticity. Maybe at a later stage, the dynamic surface tension might be studied based on the code currently developed.

Chapter 3

Molecular Dynamics

3.1 Conventional MD

Macroscopic quantities are averages over an ensemble of microscopic states. If a system is ergodic, ensemble averages are equivalent to time averages. The Molecular Dynamics method is based on this equivalence. In classical Molecular Dynamics microscopic states are generated by Hamilton's equations of motion, which are equivalent to Newton's equations (for atomic systems). Since energy is a conserved quantity, the natural ensemble simulated by Molecular Dynamics is the microcanonical one. Ergodicity then means that the system will have passed an equal number of times through every phase-space element lying on the hypersurface of constant energy.

If the potential is a continuous function of particle coordinates, the equations of motions can be solved by finite difference methods. If this is not the case as for hard spheres and square wells, collisions should be taken into account explicitly. Finite difference methods solve the equations of motion on a discrete time scale. The time step δt should be chosen such that the forces can be considered constant during one time interval. A variety of algorithms is available, which roughly fall into two classes. These are the predictor-corrector algorithms and the Verlet algorithms. Both types are reviewed by Allen and Tildesley [14]. Here we will only consider the Verlet type.

The original Verlet algorithm is a direct solution of Newton's equations. Positions at time $t + \delta t$ are calculated from positions and forces at time t and positions at time $t - \delta t$. The velocities are not necessary to propagate the system, but only in calculating the kinetic energy. Two modifications of the original algorithm are the leap-frog and the velocity-Verlet schemes.

In the leap-frog algorithm positions $\underline{r}$ and velocities $\underline{v}$ are advanced by

$$\underline{r}\left(t + \delta t\right) = \underline{r}\left(t\right) + \delta t \, \underline{v}\left(t + \tfrac{1}{2}\delta t\right),$$
$$\underline{v}\left(t + \tfrac{1}{2}\delta t\right) = \underline{v}\left(t - \tfrac{1}{2}\delta t\right) + \delta t \, \underline{a}\left(t\right), \tag{3.1}$$

with $\underline{a}$ the acceleration. To calculate quantities that require velocities at integer multiples of the time step (i.e. $t = n\delta t$), such as the kinetic energy, velocities should be calculated as

$$\underline{v}\left(t\right) = \frac{1}{2}\left[\underline{v}\left(t + \tfrac{1}{2}\delta t\right) + \underline{v}\left(t - \tfrac{1}{2}\delta t\right)\right]. \tag{3.2}$$

The velocity-Verlet algorithm stores positions, velocities and accelerations all at the same time and is given by

$$\underline{r}\left(t + \delta t\right) = \underline{r}\left(t\right) + \delta t \, \underline{v}\left(t\right) + \frac{1}{2}\left(\delta t\right)^{2} \underline{a}\left(t\right),$$
$$\underline{v}\left(t + \delta t\right) = \underline{v}\left(t\right) + \frac{1}{2}\delta t \left[\underline{a}\left(t\right) + \underline{a}\left(t + \delta t\right)\right]. \tag{3.3}$$

The velocity-Verlet scheme is attractive for reasons of storage, numerical stability and simplicity.

It should be noted that every integration algorithm leads to differences from the exact solution for very long times (due to the finite time step). This is fatal only, if we are interested in dynamic properties over large time scales. If an exact solution can be obtained for times comparable with the correlation times of interest, time correlation functions, corresponding to dynamic properties, can be calculated accurately.

If we are not interested in dynamic properties, the only requirement is to generate the microcanonical ensemble. For this purpose, we do not need the exact trajectories. Instead, energy conservation is essential and should therefore be the main test of a finite difference algorithm.

3.2 Thermostatting

The natural ensemble for Molecular Dynamics simulations, is the microcanonical ensemble. In order to simulate the canonical ensemble, we have to change the dynamics of the system. Below a comparison is made between a few important methods of constant temperature Molecular Dynamics. A more extensive review is given by Nosé [15].

3.2.1 Velocity scaling

Velocity scaling is the earliest method. It scales the velocities of all particles at each time step, in such a way that the instantaneous kinetic energy is fixed to the constant value corresponding to the desired temperature. Therefore it is called a constraint method. Since the kinetic energy should fluctuate in finite systems, constraint methods do not generate the right distribution of microscopic states in momentum space. However, this is not an important disadvantage, since properties depending on momenta only, can easily be calculated analytically. The question is, whether this particular method generates the canonical distribution in coordinate space. According to Nosé, the momentum-scaling procedure does not. In fact, the coordinate part of the generated distribution would show the same deviations from the canonical distribution as does the microcanonical distribution projected onto coordinate space. (To answer this question, we present numerical investigations in section 6.4.) If this is the case, scaling would be useless in simulating the canonical ensemble. In simulating the microcanonical ensemble, however, the procedure would be helpful in adjusting the energy E of the system to $\langle \mathcal{H} \rangle_{NVT}$. This is necessary, if one wants to compare microcanonical and canonical simulations.[1]

3.2.2 Andersen's method

In 1980 Andersen [16] was the first to propose a method that generates the canonical ensemble in phase space. In his approach, the particles change their momenta instantaneously by stochastic collisions. Particles suffer collisions the rate of which is determined by an average collision rate ν. The velocity of a particle after a collision is sampled from the Boltzmann distribution at the desired temperature. The time evolution of the system can thus be divided into a Hamiltonian part and a collisional part. Collisions change the kinetic energy of the system, as a result of which the system jumps to a hypersurface with a different energy. This is shown in figure 3.1. The canonical ensemble is obtained, if the Hamiltonian motion forces the system to pass through every point on a surface of constant energy with the same probability, i.e. if the sytem is ergodic. This demand, which is the same as for conventional microcanonical MD, is sufficient but not necessary. This is because the collisions increase the freedom of the motion in phase space.

The collision frequency ν does not affect equilibrium properties of the system. However, dynamic properties are very sensitive to this collision frequency. Therefore, it is reasonable

---

[1]Constraint methods can also be defined in terms of a Hamiltonian of an extended system. The choice of the potential of the extra variable then determines the dynamics of the system. In this respect there is a unique potential which generates the canonical ensemble in coordinate space (compare section 3.2.3).
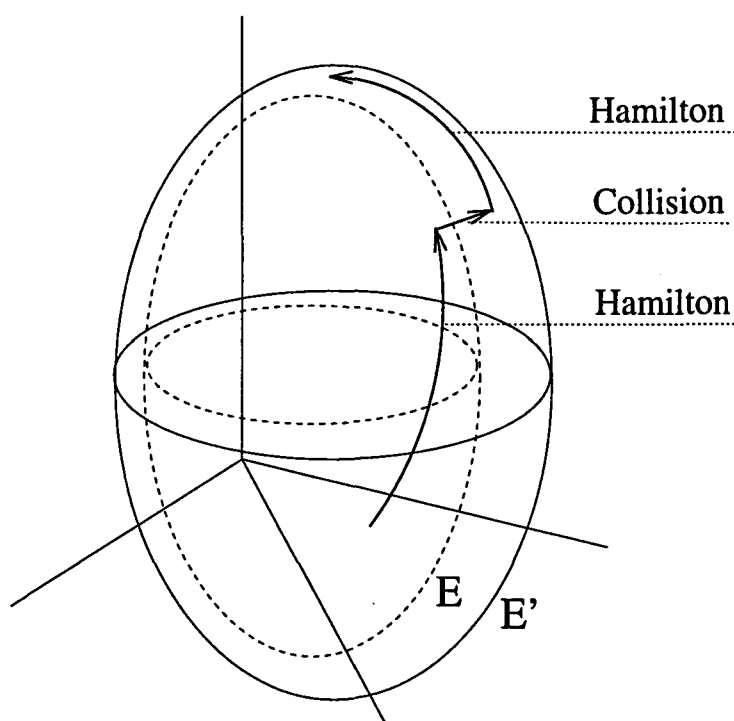
Figure 3.1: *Time evolution in phase space of a system governed by Andersen's dynamics. The motion is mostly on a surface of constant energy, but sometimes a collision forces the system to continue its motion at a different energy.*

to choose the collision frequency, so as to simulate a real fluid element subjected to energy fluctuations due to its surroundings. Consider a system of volume V consisting of N particles surrounded by a reservoir at temperature T. Suppose that the temperature of the system is $T + \Delta T$. Then the system will lose energy to the reservoir at a rate proportional to the thermal conductivity κ and the temperature difference ΔT. By dimensional considerations, the rate of heat loss is shown to be $a\kappa \Delta T V^{1/3}$, where a is a dimensionless constant dependent on the shape of the system. This energy loss rate should be equal to $3N\nu k_B \Delta T/2$, the loss of kinetic energy due to collisions. So ν can be related to the thermal conductivity by

$$\nu = \frac{2a\kappa}{3k_B \rho^{1/3} N^{2/3}},\tag{3.4}$$

where $\rho = N/V$. A crude estimation of ν follows from the consideration of a system containing only one particle. In this case it is reasonable to set ν equal to the actual collision frequency ν_c for a particle. Elimination of κ then leads to the relation $\nu = \nu_c/N^{2/3}$. For a large number of particles, ν is much smaller than the actual collision frequency. Therefore, the Hamiltonian motion is dominant and only infrequently a particle will suffer a collision.

3.2.3 Nosé-Hoover

Andersen's method has the disadvantage that the evolution of the system is governed by stochastic processes. Nosé [17] proposed a method that is fully deterministic. His so-called extended system method introduces an additional degree of freedom s with associated momentum p_s, which acts as an external system on the physical system. Also virtual variables are introduced for the particle coordinates, momenta and for time. The transformation from real to virtual variables can be interpreted as a time-scaling transformation where the scaling factor is s. Therefore the virtual coordinates are equal to the real ones, while the virtual momenta differ from the real momenta by a factor s. The extended system is then described by a Hamiltonian, where the choice of the potential dependence on the variable s turns out to be essential. Since we are dealing with canonical equations of motion in the virtual variables, energy is conserved in these variables. Transforming back to real variables, this virtual microcanonical ensemble changes into the canonical ensemble in real phase space, only for a particular choice for the potential dependence on s. Nosé shows that this dependence should be chosen logarithmic. In his analysis, effects of conservation of total momentum, which are of the order $1/N$, are neglected.[2]

Hoover [18] later pointed out that the only significant variable for the external heat bath is a friction coefficient $\zeta = sp_s/Q$, where Q is the mass for the motion of s. Using this variable the time-scaling can be interpreted as a frictional effect. The resulting equations, constituting what is now know as the Nosé-Hoover thermostat, become [19]

$$\begin{aligned}
\frac{d\underline{r}_i}{dt} &= \underline{v}_i, \\
\frac{d\underline{v}_i}{dt} &= -\frac{1}{m_i}\frac{\partial \mathcal{U}}{\partial \underline{r}_i} - \zeta \underline{v}_i, \\
\frac{d\zeta}{dt} &= \frac{1}{Q}\left(\sum_i m_i v_i^2 - g k_B T\right), \\
\frac{d\ln s}{dt} &= \zeta.
\end{aligned}\tag{3.5}$$

The quantity g is the number of degrees of freedom $3N - 3$. The first three equations form a closed set. Note that in the second equation an additional force is introduced, which has a

---

[2]Note that in a simulation box with periodic boundary conditions, the total angular momentum is not conserved.

thermostatting effect. The last equation, however, is very useful to check for programming errors and to estimate the accuracy of the integration algorithm. Indeed, s is necessary in calculating the conserved quantity

$$\mathcal{H}_{\text{Nosé}} = \mathcal{H} + \frac{1}{2}Q\zeta^2 + gk_BT\ln s. \tag{3.6}$$

This quantity is not a Hamiltonian, since the equations of motion are not canonical.

The traditional leap-frog algorithm extended to Nosé-Hoover MD, works well and samples the canonical distribution correctly if the quality factor Q is chosen appropriately [20]. This quality factor is defined in terms of the thermostat time constant τ as $Q = gk_BT\tau^2$. This time constant in combination with the time step should be chosen such that $\mathcal{H}_{\text{Nosé}}$ is constant to within the required accuracy.

Nosé-Hoover MD generates the canonical distribution if the ensemble averages and trajectory averages are equal, i.e. the system is ergodic. Practically this means that the system should be sufficiently chaotic. A notable exception is the single harmonic oscillator [18]. Difficulties are also expected for other small or stiff systems. Generalizations from a single thermostat variable to a chain of variables might help in these cases [21].

Of course the Nosé-Hoover thermostat changes the time-dependent properties of the system. Studying time-dependent properties is only allowed, if the thermostat time constant τ corresponds to the time constant governing the energy fluctuations in a real system. This demand is equivalent to the demand on the collision frequency ν in Andersen's method. We will not be studying time-dependent properties, so a check on the conservation of $\mathcal{H}_{\text{Nosé}}$ will be sufficient.

Chapter 4

Derivatives of thermodynamic quantities

4.1 Introduction

In general the partition function of a system is difficult to obtain from a simulation. The reason is that the partition function involves a summation over microscopic states instead of an averaging. Derivatives of the partition function with respect to the fixed parameters of the ensemble, respectively N, V, E in the microcanonical ensemble and N, V, T in the canonical, contain important information of the system. These derivatives are available from simulation, because they can be written in terms of averages over microscopic states. Starting from a well-known system, the partition function of the system of interest can then be found by integration of these derivatives.

Since in conventional Molecular Dynamics the microcanonical ensemble is simulated, whereas the canonical ensemble is more relevant to the present problem, we will treat them both in the following sections. In this thesis we will focus on derivatives with respect to the important length scales of the system. Derivatives with respect to the other fixed parameters of the ensemble can be treated completely analogously.

Neglecting surface effects, for atomic one-component systems the only dimension of importance is the total volume of the system, since the system is isotropic. The integration over particle coordinates is limited to the volume of the system. This volume dependence can be removed by a transformation invented by Green [22], which is given by

$$\underline{r}_i = V^{1/3}\, \underline{r}'_i, \tag{4.1}$$

This transformation is commonly used (see e.g. McQuarrie [23]). It introduces a Jacobian V^N in coordinate space. For non-isotropic systems, such as solids, length scales in different directions should be treated separately.

We will also be regarding systems that can be characterized not only by their volumes, but also by a particular interfacial area A. For these systems the microcanonical and canonical ensemble refer to systems at constant N, V, A, E and N, V, A, T respectively. We will only be considering flat interfaces and take the z-direction perpendicular to the interface. Area derivatives at constant volume can then be treated by the following transformation [24]:

$$
\begin{aligned}
x_i &= A^{1/2}\, x'_i, \\
y_i &= A^{1/2}\, y'_i, \\
z_i &= \frac{V}{A}\, z'_i.
\end{aligned}
\tag{4.2}
$$

Note that this transformation does not introduce a Jacobian different from unity, in contrast to transformation 4.1.

4.2 Derivatives in the microcanonical ensemble

As stated in the first chapter the phase-space density of the microcanonical ensemble is proportional to $\delta\left(E-\mathcal{H}\right)$, with the Hamiltonian depending on particle coordinates and impulses. Integration of this density gives the function $\omega\left(N,V,E\right)$, which is the derivative with respect to E of the phase-space volume $\Omega\left(N,V,E\right)$. These functions are given by

$$
\begin{aligned}
\Omega\left(N,V,E\right) &= \frac{1}{C}\int d\underline{r}^N d\underline{p}^N \Theta\left(E-\mathcal{H}\right), \\
\omega\left(N,V,E\right) &= \frac{1}{C}\int d\underline{r}^N d\underline{p}^N \delta\left(E-\mathcal{H}\right),
\end{aligned}
\tag{4.3}
$$

where $\Theta\left(x\right)$ is the unit step function, defined as

$$
\Theta\left(x\right) = \begin{cases} 1 & \text{if } x > 0 \\ 0 & \text{otherwise.} \end{cases}
\tag{4.4}
$$

Averages of microscopic quantities $\mathcal{B}\left(\underline{r}^N,\underline{p}^N\right)$ depending on particle coordinates and momenta are then written as

$$
\langle\mathcal{B}\rangle = \frac{1}{\omega C}\int d\underline{r}^N d\underline{p}^N \mathcal{B}\,\delta\left(E-\mathcal{H}\right).
\tag{4.5}
$$

In order to obtain thermodynamic properties, we have to define the entropy S of the system. In the microcanonical ensemble there is some ambiguity in this definition. Two possibilities are, among others, to define the entropy as $k_B\ln\Omega$ or $k_B\ln\omega$. These definitions are in agreement to order $1/N$. Following Pearson, we will start from the first definition and apply a Laplace-transform technique to obtain expressions for thermodynamic derivatives.

The integral definitions of Ω, ω and $\langle\mathcal{B}\rangle$ can be rewritten in a more suitable form by taking the Laplace transform with respect to energy. Since the Hamiltonian is separable in coordinates and momenta, the momenta integrals can be performed. Here it is necessary that $\mathcal{B}$ is a function of particle coordinates only, which we will assume in the following. Inverse transformation then leads to the following expressions:

$$
\begin{aligned}
\Omega\left(N,V,E\right) &= \frac{1}{C_0\Gamma\left(3N/2+1\right)}\int d\underline{r}^N \left(E-\mathcal{U}\right)^{3N/2}\Theta\left(E-\mathcal{U}\right), \\
\omega\left(N,V,E\right) &= \frac{1}{C_0\Gamma\left(3N/2\right)}\int d\underline{r}^N \left(E-\mathcal{U}\right)^{3N/2-1}\Theta\left(E-\mathcal{U}\right), \\
\langle\mathcal{B}\rangle &= \frac{1}{\omega C_0\Gamma\left(3N/2\right)}\int d\underline{r}^N \mathcal{B}\left(E-\mathcal{U}\right)^{3N/2-1}\Theta\left(E-\mathcal{U}\right),
\end{aligned}
\tag{4.6}
$$

where $\Gamma\left(n\right)$ is the gamma function and the new constant of proportionality is related to the old one by $1/C_0 = \left(2\pi m\right)^{3N/2}/C$. (The potential energy $\mathcal{U}$ depends on particle coordinates only.)

Using these expressions, the temperature, which is defined by $1/T = \left(\partial S/\partial E\right)_{NV}$, can easily be obtained as

$$
k_B T = \frac{\Omega}{\omega} = \frac{2}{3N}\langle E-\mathcal{U}\rangle = \frac{2}{3N}\langle\mathcal{K}\rangle.
\tag{4.7}
$$

This is a direct illustration of the equipartition theorem.

We will now turn to the question of how to deal with derivatives with respect to volume. Integration over particle coordinates is limited to the volume of the system. This dependence is

removed by Green's change of variables. In the microcanonical ensemble the pressure is defined by $p = -(\partial E/\partial V)_{NS} = T(\partial S/\partial V)_{NE}$ and can be written as

$$p = \frac{1}{\omega}\frac{\partial \Omega}{\partial V} = \frac{N}{V}k_B T - \left\langle\frac{\partial \mathcal{U}}{\partial V}\right\rangle. \tag{4.8}$$

In this expression the first term is the ideal gas contribution or kinetic term. The second term is a result of interactions between the particles. For pair-wise additive interactions it can be expressed in the virial function $\mathcal{W}$ (see appendix A). Equation 4.8 is then referred to as the virial theorem.

In general, the derivative of an average quantity can be written as

$$\frac{\partial\langle\mathcal{B}\rangle}{\partial V} = -\left(\frac{3N}{2}-1\right)\left\langle\delta\mathcal{B}\,\delta\left(\frac{1}{\mathcal{K}}\frac{\partial\mathcal{U}}{\partial V}\right)\right\rangle + \left\langle\frac{\partial\mathcal{B}}{\partial V}\right\rangle. \tag{4.9}$$

In this expression we can substitute for $\mathcal{B}$ the potential energy $\mathcal{U}$. Since total energy is kept constant while differentiating with respect to volume, we automatically find an expression for the dependence of kinetic energy on volume, i.e. $\partial\langle\mathcal{K}\rangle/\partial V = -\partial\langle\mathcal{U}\rangle/\partial V$.

The surface tension γ is defined analogously to the pressure as $(\partial E/\partial A)_{NVS} = -T(\partial S/\partial A)_{NVE}$. Using the Laplace transform technique this can be written as

$$\gamma = -\frac{1}{\omega}\frac{\partial\Omega}{\partial A} = \left\langle\frac{\partial\mathcal{U}}{\partial A}\right\rangle. \tag{4.10}$$

Note that there is no kinetic term here.

4.3 Derivatives in the canonical ensemble

For volume derivatives in the canonical (and also the grand canonical ensemble) we refer to Gray and Gubbins [25], where a detailed treatment can be found. In the canonical ensemble the pressure is defined as the volume derivative of the free energy $p = -(\partial F/\partial V)_{NT}$. The free energy is related to the partition function by $Z = \exp(-\beta F)$. The volume dependence of the partition function is fully described by the configuration integral

$$\int d\underline{r}^N e^{-\beta\mathcal{U}}. \tag{4.11}$$

Using Green's transformation 4.1, we can remove the volume dependence of the integration boundaries, resulting in

$$p = \frac{N}{\beta V} - \left\langle\frac{\partial\mathcal{U}}{\partial V}\right\rangle. \tag{4.12}$$

So we find the same expression as in the microcanonical ensemble. This should always be the case for averages, as explained in chapter 2.

Now consider the volume derivative of the average of an arbitrary quantity $\mathcal{B}$. Again using the transformation due to Green, we can write

$$\frac{\partial\langle\mathcal{B}\rangle}{\partial V} = -\beta\left\langle\delta\mathcal{B}\,\delta\left(\frac{\partial\mathcal{U}}{\partial V}\right)\right\rangle + \left\langle\frac{\partial\mathcal{B}}{\partial V}\right\rangle. \tag{4.13}$$

Taking for the quantity $\mathcal{B}$ the potential energy, we obtain an expression for $\partial\langle\mathcal{U}\rangle/\partial V$. Note that in the canonical ensemble $\partial\langle\mathcal{K}\rangle/\partial V$ equals zero.[1] Using the relation between free energy

---

[1] This is not the case in the grand canonical ensemble due to the variable particle number.

and internal energy $F = \langle \mathcal{H} \rangle - TS$, the volume dependence of the entropy S in the canonical ensemble is obtained as

$$T \frac{\partial S}{\partial V} = \frac{N}{\beta V} - \beta \left\langle \delta \mathcal{U} \, \delta \left(\frac{\partial \mathcal{U}}{\partial V} \right) \right\rangle. \tag{4.14}$$

This quantity can be related to the thermal pressure coefficient via the Maxwell relation

$$\left(\frac{\partial S}{\partial V} \right)_{NT} = \left(\frac{\partial p}{\partial T} \right)_{NV}, \tag{4.15}$$

which can be obtained by differentiating the free energy with respect to both volume and temperature in different order.

We will now treat area derivatives in the canonical ensemble. The derivative of the free energy with respect to the interfacial area is called the surface tension of this interface, i.e. $\gamma = (\partial F / \partial A)_{NVT}$. Note again the sign difference with the definition of the bulk pressure. Where pressure has the tendency to increase the volume of a system, surface tension tends to minimize the interfacial area. Using the transformation 4.2, we find for the surface tension the same expression as in the microcanonical ensemble, as we expected.

The area derivative of an arbitrary average can be written as

$$\frac{\partial \langle \mathcal{B} \rangle}{\partial A} = -\beta \left\langle \delta \mathcal{B} \, \delta \left(\frac{\partial \mathcal{U}}{\partial A} \right) \right\rangle + \left\langle \frac{\partial \mathcal{B}}{\partial A} \right\rangle. \tag{4.16}$$

Again taking for $\mathcal{B}$ the potential energy, the covariance can be related to the change in entropy by

$$T \frac{\partial S}{\partial A} = -\beta \left\langle \delta \mathcal{U} \, \delta \left(\frac{\partial \mathcal{U}}{\partial A} \right) \right\rangle, \tag{4.17}$$

where we used the fact that the average kinetic energy does not depend on A. This quantity can be helpful in studying phase transitions due to surface properties. It can be related to the 'thermal surface tension coefficient' by

$$\left(\frac{\partial S}{\partial A} \right)_{NVT} = - \left(\frac{\partial \gamma}{\partial T} \right)_{NVA}. \tag{4.18}$$

Stability criteria of interfaces involve the second derivative of the free energy with respect to the interfacial area. As mentioned in the introductory chapter, this can be expressed by the surface elasticity, which was first defined by Gibbs as $\varepsilon = (\partial \gamma / \partial \ln A)_{NVT}$. Taking for $\mathcal{B}$ in equation 4.16 the quantity $\partial \mathcal{U} / \partial A$, we find for the surface elasticity

$$\varepsilon = A \left(-\beta \left\langle \left(\delta \left(\frac{\partial \mathcal{U}}{\partial A} \right) \right)^2 \right\rangle + \left\langle \frac{\partial^2 \mathcal{U}}{\partial A^2} \right\rangle \right). \tag{4.19}$$

Chapter 5

Error estimation

5.1 Introduction

We use simulation as a computational approach to a physical problem. Typically, this involves breaking up differential equations into finite-difference equations, restricting infinite time integrals to finite ones, etc. In order to quantify the errors involved, we discuss in this chapter the mathematics surrounding our error estimation. It should be realised that as the Gibbs elasticity is a fluctuation quantity, we have to discuss error estimates for nonlinear quantities (section 5.3) which are not readily found in literature as are the conventional techniques for averages (section 5.2).

5.2 The blocking method

The problem in estimating errors in averaged properties, is the time correlation of the data. Allen and Tildesley [14] describe a procedure which is known as batching of the data. Batching in this sense means dividing the data in blocks of the same length. The statistics of these blocks then give a way of determining the so-called efficiency parameter, which is a measure of the time correlation. To obtain the error in an averaged quantity this efficiency parameter should be studied as a function of block size. Since this is an elaborate operation, we will now focus on an alternative procedure called the blocking method [26] .

The blocking method transforms the original data series $\{x_1, .., x_n\}$ into half as large a data series $\{x'_1, .., x'_{n'}\}$, where

$$
\begin{aligned}
x'_i &= \frac{1}{2}(x_{2i-1} + x_{2i}), \\
n' &= \frac{n}{2}.
\end{aligned}
\tag{5.1}
$$

Repeated application of this transformation, creates a number of new series. The average m and variance of the average $\sigma^2(m)$ of the data is invariant under this transformation. Therefore, no relevant information is lost in this transformation of the data series to half as large a series. Not only is nothing lost, but something is gained: Flyvbjerg and Petersen show that an estimate for $\sigma^2(m)$ is given by

$$
\frac{\sigma^2(x)}{n-1},
\tag{5.2}
$$

where $\sigma^2(x)$ is the variance of the data series

$$
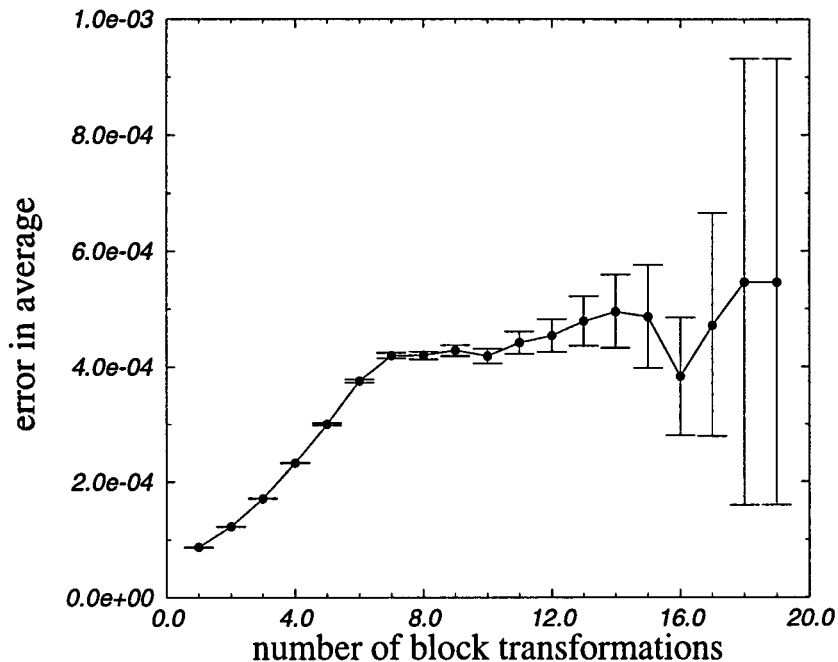\sigma^2(x) = \frac{1}{n}\sum_{i=1}^{n}(x_i - m)^2.
\tag{5.3}
$$

Figure 5.1: *Error in* $\langle \mathcal{U}/N \rangle$ = −4.340 *as a function of the number of block transformations applied for a Nosé-Hoover simulation at* ρ^* = 0.835, T^* = 1.0 *and* N = 500. *The value at the plateau gives the best estimate.*

Because of the time correlation in the data, we should study this estimate as a function of the number of transformations applied. The number of transformations can both be too small, causing the resulting series to still be time correlated, or too large, causing the resulting series to be too small to obtain good statistics. Fortunately there is an optimum in between, which gives a good estimate of the error in the average $\sigma\,(m)$ and even an uncertainty interval around this error:

$$\sigma\,(m) \approx \sqrt{\frac{\sigma^2\,(x)}{n-1}} \left(1 \pm \frac{1}{\sqrt{2\,(n-1)}} \right). \tag{5.4}$$

A typical result is shown in figure 5.1.

5.3 The jackknife method

The blocking method works well for averages. However the quantities we are interested in, involve variances and covariances. To make an error estimation of these quantities, we have to use different procedures, such as the jackknife or the bootstrap method [27]. We will only be considering the jackknife method here.

For time uncorrelated data this method makes a set of n new data series by omitting each data point from the original series. For correlated data a block of m data points should be removed, resulting in n/m new series. For each of this new series, we can calculate the quantities of interest. In our case this can be eiter an average, a variance or a covariance. Statistics on these quantities give us an estimate of the standard error in them. Time correlation again forces

us to study these estimates as a function of the block size m. If we now take this block size to be an increasing power of two, we can for averages make a full comparison with the blocking method. We will apply the jackknife method in the error estimation of the simulations described in the following chapters.

Chapter 6

Simulation of the Lennard-Jones liquid

6.1 Introduction

In the next chapter, we will discuss the physical system that we are interested in. It consists of two liquids. Particles of equal identity attract each other by a Lennard-Jones potential. Particles of different identity repel each other. Surfactants are build by joining some particles of different identity by a spring-like potential. This system should provide a simple generic model of a liquid-liquid interface. It has proved useful for this goal in numerous studies in the past (Telo da Gama and Gubbins [28], Smit [29] and Karaborni et al. [30]).

The Lennard-Jones liquid has been studied since the early days of simulation. We will not try to give an overview on a subject as extensive as this. Our main interest is not in the thermodynamics of the Lennard-Jones liquid, but in phenomena occurring at the interface of two immiscible Lennard-Jones liquids. Therefore, in this chapter we will focus on those topics that are of importance to simulation techniques, instead of making a quantitative description of the Lennard-Jones liquid in terms of equations of states and dynamics. We also add a discussion of different ensembles (section 6.4) and the calculation of fluctuations, exemplified by the melting transition (section 6.5).

6.2 The effective pair potential

In general, interactions between atoms of simple liquids can adequately be described in terms of pair potentials.[1] Three-body ·interactions are undoubtedly significant at liquid densities. Nevertheless they are only rarely included in computer experiments, since any calculation involving a sum over triplets of atoms will be very time-consuming. Fortunately the average three-body effects can be partially included in an effective pair potential. Four-body and higher interactions can be fully neglected.

In simple liquids the pair potential can be separated in a short-range repulsion and an attraction of longer range. For reasons of mathematical convenience, the short-range repulsive interaction is usually represented by an inverse power law, i.e. r^{-n}, with n in the range 9 to 15. For rare-gas atoms the leading term in the attractive interaction describes the dipole-induced dipole interaction, which varies as r^{-6}. Higher-order terms are generally negligible. The 12-6

---

[1]An explicit treatment of pair potentials is given in appendix A.

Lennard-Jones potential, obtained by taking $n = 12$, is of the form

$$u^{LJ}(r) = 4\epsilon \left[\left(\frac{\sigma}{r}\right)^{12} - \left(\frac{\sigma}{r}\right)^6 \right],$$ (6.1)

where σ is the collision diameter and ϵ the depth op the potential well. The Lennard-Jones potential gives an adequate description of the interaction between pairs of rare-gas atoms and also of quasispherical molecules, such as CH_4.

If interactions between particles are completely specified by a few parameters, it is useful to introduce reduced units. For the Lennard-Jones potential, these parameters are σ and ϵ. Reduced lengths and energies are thus expressed in units of σ and ϵ respectively. In chapter 2 we already introduced the reduced density $\rho^* = \rho\sigma^3$ and temperature $T^* = k_B T/\epsilon$. Similarly, pressure reduces to $p^* = p\sigma^3/\epsilon$ and surface tension to $\gamma^* = \gamma\sigma^2/\epsilon$. Considering systems consisting of just one particle type, another parameter that enters in the equations of motion is the mass of a particle. In reduced units this is taken as the unit of mass, so that impulses and velocities as well as forces and accelerations are numerically equal. Using reduced units, time will be saved in the simulation, since parameters as σ, ϵ and m do not appear explicitly. Moreover, simulations in reduced units have the property to be generic for a class of systems, in this case Lennard-Jones systems.

For liquid argon the effective pair potential can be described by a Lennard-Jones potential with $\epsilon/k_B = 119.8$ K and $\sigma = 0.341$ nm. Using these values and an atomic mass $m = 39.948$ u, a reduced time unit corresponds to 2.2 ps. A typical value for the time step used in the integration of the equations of motion, is 0.005 in reduced units. Using $t^* = (m\sigma^2/\epsilon)^{-1/2} t$, this is of the order 10 fs.

Computer simulations are performed on finite systems. Finite systems show surface effects, which are unwanted in studying bulk properties. This problem can be overcome by the introduction of periodic boundary conditions. In a periodic system, the container walls of the simulation box are removed. Instead, the original box is replicated throughout space, forming an infinite lattice. Since all boxes are the same, a particle leaving the central box through one face, will enter the central box as one of its periodic images through the opposite face. A periodic system is a good model of the macroscopic system which it represents, if the range of interaction is short compared to the size of the box. For Lennard-Jones particles simulated in a cubic box with periodic boundaries, a size of 6σ suffices. Still not every phenomenon can be studied using a periodic setup. Density waves with a wavelength larger than the size of the simulation box are suppressed. It is therefore impossible to simulate a liquid close to the gas-liquid critical point, where the range of critical fluctuations is macroscopic. Furthermore, suppression of fluctuations causes first order phase transitions to show characteristics of higher order transitions.

It is impossible to include all interactions between particles, regardless of the box they are in. In the minimum-image convention, a particle in the central box interacts with the closest periodic images of the other $N-1$ particles. The calculation of the potential energy then involves $N(N-1)/2$ terms. To reduce this number, a further approximation is made. For short-range forces, a spherical cut-off can be introduced. For a Lennard-Jones pair potential a typical cut-off radius is $r_c = 2.5\sigma$.

Applying a cut-off introduces a discontinuity in the potential and the forces at the cut-off sphere. Since the equations of motion are solved using a finite time step, these discontinuities introduce some difficulties. We can overcome these problems by slightly changing the potential. If we want the total energy to be conserved in a microcanonical simulation, it suffices to shift the potential by its value in r_c. Then the forces still show a discontinuity, which is removed by making the potential differentiable at $r = r_c$. In our simulations we have used a special-purpose potential, which is continuous up to the second derivative with respect to r at the cut-off. The reason for this is that the surface elasticity involves this second derivative.

There is some freedom in the different shifting procedures. For instance we could choose r as
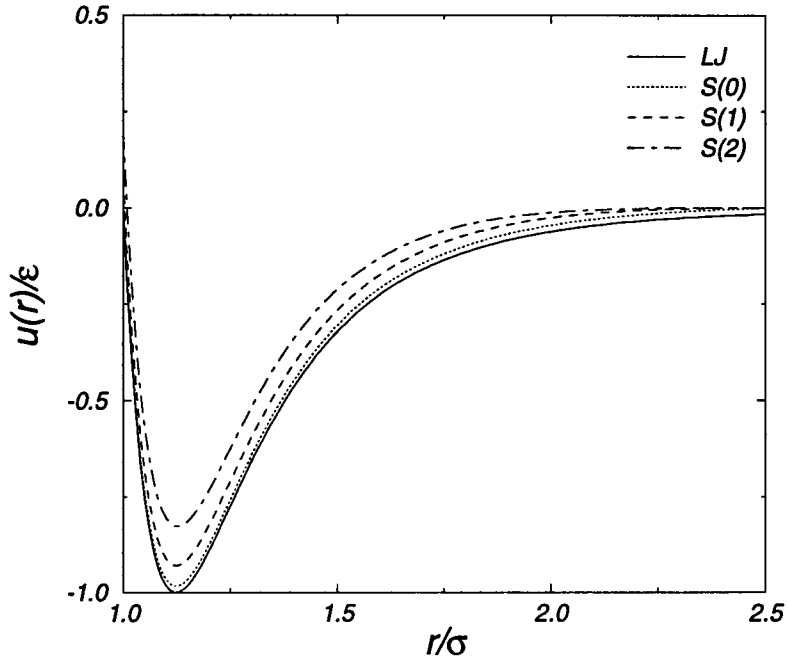
Figure 6.1: *The potentials $u^{S(m)}$.*

the principal variable and shift the potential to order m, yielding

$$u^{S(m)}(r) = u^{LJ}(r) - \sum_{k=0}^{m} \left[\frac{d^k u^{LJ}(r)}{dr^k} \right]_{r_c} \frac{(r - r_c)^k}{k!} \qquad (6.2)$$

for $r \leq r_c$. The term with $k = 1$ involves r, which is obtained by taking the square root of $x^2 + y^2 + z^2$. This is a time-consuming operation. We can avoid the square root evaluations by taking $r^2/2$ instead of r as the principal variable. The potential is then shifted to order m, according to

$$\widetilde{u}^{S'(m)}\left(\tfrac{1}{2}r^2\right) = \widetilde{u}^{LJ}\left(\tfrac{1}{2}r^2\right) - \sum_{k=0}^{m} \left[\frac{d^k \widetilde{u}^{LJ}\left(\tfrac{1}{2}r^2\right)}{d\left(\tfrac{1}{2}r^2\right)^k} \right]_{\tfrac{1}{2}r_c^2} \frac{\left(\tfrac{1}{2}r^2 - \tfrac{1}{2}r_c^2\right)^k}{k!}, \qquad (6.3)$$

with $\widetilde{u}\left(r^2/2\right) = u(r)$. These potentials are shown in figures 6.1 and 6.2.

As can be seen the potentials shifted in $r^2/2$ show a smaller deviation from the unshifted Lennard-Jones potential than the ones shifted in r. We have chosen $u^{S'(2)}$ for the interatomic potential.

In a Molecular Dynamics simulation, the calculation of the interatomic forces is the most time-consuming part. For this reason, we implemented a table equidistant in r^2 for the potential. This table is constructed at the beginning of a simulation. During the simulation, values of r_{ij}^2 are calculated for pairs of atoms i and j. The potential is then found by interpolation from the table. We used the Newton-Gregory forward-difference method [14]. (Linear interpolation will be sufficient for a larger table.) The length of an interval was chosen to be $\sigma^2/100$, yielding with a cut-off radius $r_c = 2.5\sigma$ a table of 625 intervals.
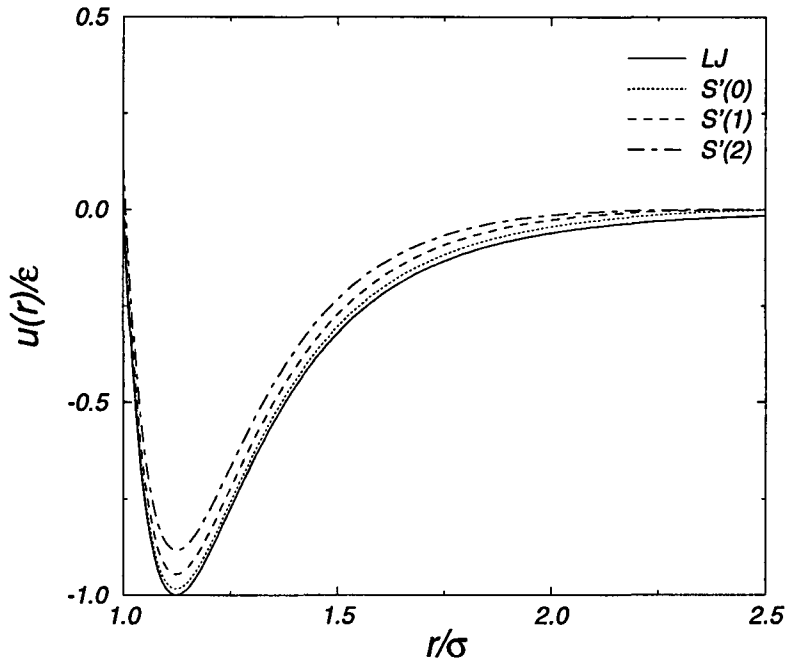
Figure 6.2: *The potentials $u^{S'(m)}$.*

We can accelerate the force calculation even more by maintaining a list of the neighbours of each particle in the central box. We used the Verlet neighbour list where the cut-off sphere is surrounded by a skin, giving a larger sphere of radius r_l (see figure 6.3). Particles that are within a sphere of radius r_l from a certain particle, are called the neighbours of this particular particle.

At the beginning of the program, the neigbour list is created. In the force routine, we then only have to examine the neighbours of each particle and check whether they are in the cut-off sphere. The neigbour list is updated automatically, depending on the displacements of the particles since the last update. In principle, the list should be updated when the sum of the two largest displacements exceeds $r_l - r_c$. We used a slightly different criterium, namely that, when the square of the largest displacement in x-, y- or z-direction exceeds $(r_l - r_c)^2/3$, the list is updated.

For Lennard-Jones liquids, a typical value of r_l is 2.7σ, which corresponds to an update interval of 10-20 time steps. For systems consisting of 500 particles or more, the size of the neighbour list per particle is approximately constant. The time spent in the force calculation is thus reduced from being proportional to N^2 in the original minimum image convention to being proportional to N.

6.3 Initialisation and equilibration

Given an initial state in phase space, we now have a scheme to obtain the microscopic states our system will pass through. The choice of the initial state should not affect macroscopic quantities. One way of constructing an initial structure is to place the particles at random in the simulation box. For hard-core systems, the problem then arises that the configuration thus obtained may contain unphysical overlaps. The corresponding large forces cause difficulties in
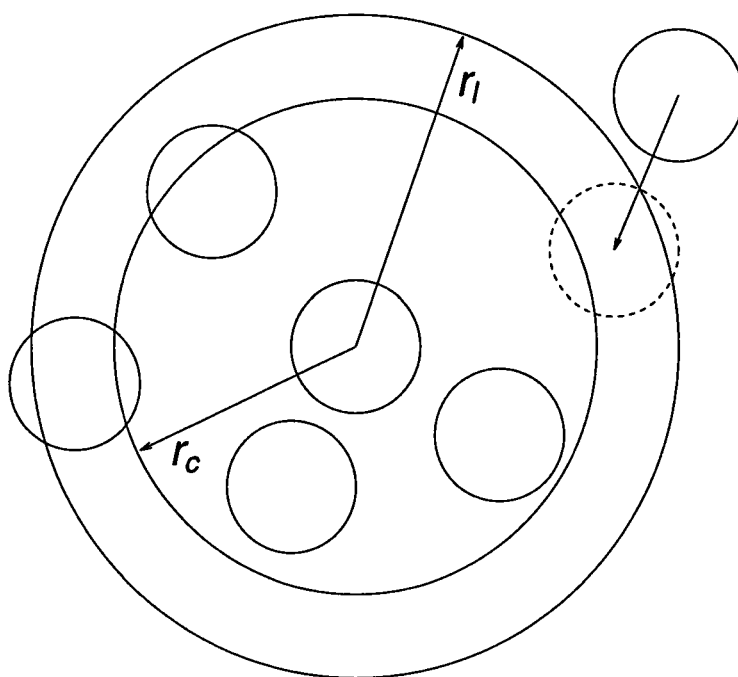
Figure 6.3: *The cut-off sphere, surrounded by the Verlet neighbour skin; only particles within the cut-off sphere interact with the central particle; if a particle enters the outer sphere, the neighbour list should be updated.*
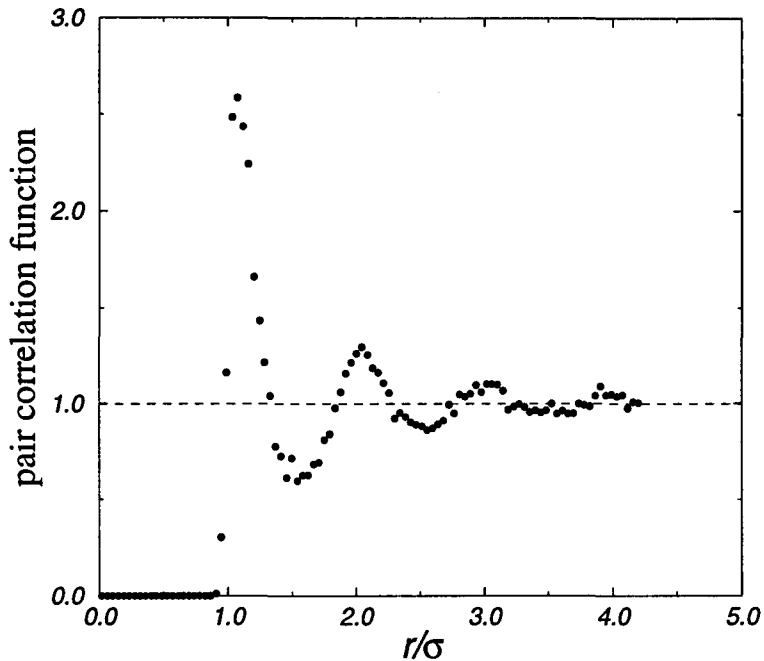
Figure 6.4: *Pair correlation function for $\rho^* = 0.83$ and $T^* = 1.0$, using 500 particles.*

solving the differential equations of motion.

For this reason, a different procedure is followed, where the initial configuration is on a Bravais lattice. Using a cubic simulation box, natural choices for this lattice are the cubic lattices. Usually the face-centred cubic lattice is chosen. Since a unit cell of the f.c.c. lattice contains 4 lattice points, the total number of particles should be chosen $4M^3$ with M a positive natural number. In our simulations, we have chosen M to be 5, corresponding to 500 particles. The initial velocities are sampled randomly from the Maxwell-Boltzmann velocity distribution at the desired temperature, corrected in such a way that there is no total momentum.

The initial state of the system is obviously not characteristic for the system in equilibrium. Therefore the system will equilibrate from the initial state during the first period of the simulation. The most sensitive indicators of the length of this equilibration period are structural properties. In the case of atomic systems these are described by the pair correlation function defined by

$$g(r) = \frac{V}{N^2} \left\langle \sum_i \sum_{j \neq i} \delta \left(\underline{r} - \underline{r}_{ij} \right) \right\rangle. \tag{6.4}$$

This definition is useful in computer experiments, where it is approximated by a histogram. We have calculated the equilibrium pair correlation function from the configuration at the end of a simulation. A typical result is shown in figure 6.4. A more accurate correlation can be found by averaging over time.

Another guideline in determining the equilibration length is the behaviour of energy and pressure. The drift that these quantities show during equilibration should vanish in equilibrium. This is only a minimal criterium. A typical behaviour of energy and pressure during equilibration is shown in figure 6.5. Here we used the Nosé-Hoover thermostat with a time constant $\tau = 0.01$. In fact, we will always use this value in this thesis. For our simulations we used an equilibration
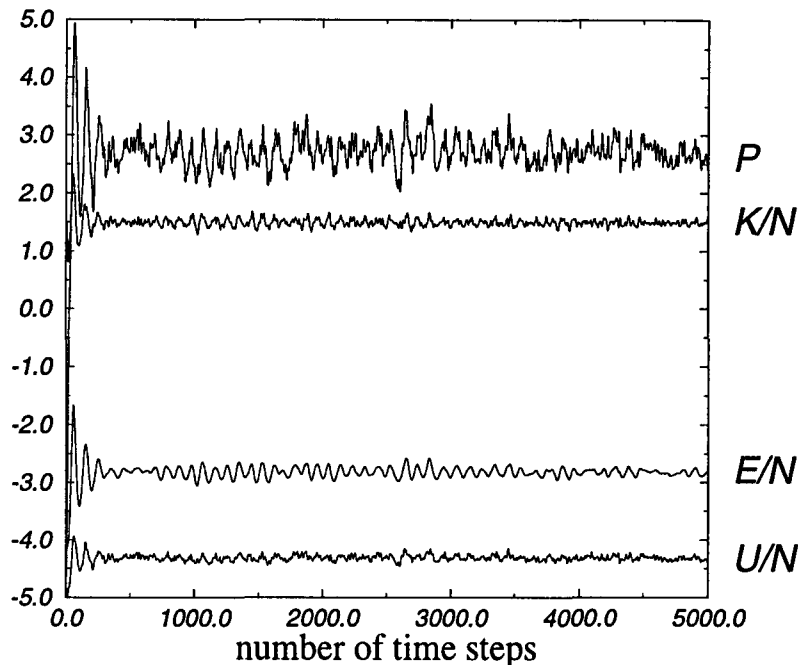
Figure 6.5: *Initialisation run of a system of 500 particles at* $\rho* = 0.83$ *and* $T^* = 1.0$, *using the Nosé-Hoover thermostat with time constant* $\tau = 0.01$.

time of 5000 time steps.

6.4 Velocity scaling compared to Nosé-Hoover

We simulated a Lennard-Jones system of 500 particles at a number density $\rho^* = 0.835$. Three different simulations were performed, two of which at a temperature $T^* = 1.0$ and the third at a constant energy per particle $E/N = \langle \mathcal{H}/N \rangle_{NVT} = -2.846$.

The first constant-temperature simulation involved a velocity-scaling procedure as described in subsection 3.2.1. The equations of motions were integrated using the velocity-Verlet algorithm described in section 3.1. In figure 6.6 the initialisation run for this simulation is shown. The kinetic energy is artificially held constant at each time step, generating the wrong distribution in momentum space.

The second constant-temperature simulation was performed using the Nosé-Hoover equations of motion. These were integrated using the leap-frog algorithm. A comparison between the three simulations is made in table 6.4. The Nosé-Hoover thermostat produces not only a kinetic energy of $3k_BT/2$ per particle, but also a variance $< \delta\left(\mathcal{K}/N\right)^2 >_{NVT} = 3\left(k_BT\right)^2/(2N)$. Together with the conservation of $\mathcal{H}_{\text{Nosé}}$, which we checked, this is a reason to trust the algorithm. Comparing the fluctuations in the potential energy and the pressure, we can conclude that the velocity-scaling procedure is more close to the Nosé-Hoover result than the microcanonical simulation.
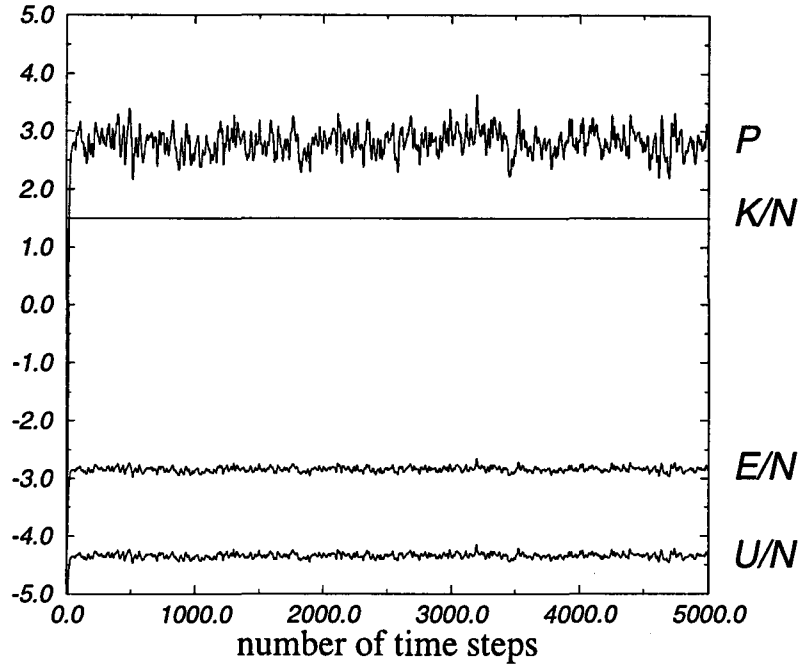
Figure 6.6: *Initialisation run of a system of 500 particles at $\rho^* = 0.835$ and $T^* = 1.0$, using the velocity-scaling procedure and the velocity-Verlet algorithm.*

	scaling	Nosé-Hoover	NVE
$\langle \mathcal{H}/N \rangle$	-2.841	-2.846	-2.846
$\langle \mathcal{K}/N \rangle$	1.497	1.494	1.494
$\langle \mathcal{U}/N \rangle$	-4.338	-4.340	-4.340
$\langle \mathcal{P} \rangle$	2.82	2.81	2.81
$< \delta\left(\mathcal{H}/N\right)^2 >$	$1.9\ 10^{-3}$	$5.0\ 10^{-3}$	$\sim O\left(10^{-8}\right)$
$< \delta\left(\mathcal{K}/N\right)^2 >$	$\sim O\left(10^{-11}\right)$	$3.0\ 10^{-3}$	$1.2\ 10^{-3}$
$< \delta\left(\mathcal{U}/N\right)^2 >$	$1.9\ 10^{-3}$	$2.0\ 10^{-3}$	$1.2\ 10^{-3}$
$< \delta\left(\mathcal{P}\right)^2 >$	$4.6\ 10^{-2}$	$4.8\ 10^{-2}$	$2.4\ 10^{-2}$
$\dfrac{<\delta(\mathcal{U}/N)\delta\mathcal{P}>}{\sqrt{<\delta(\mathcal{U}/N)^2><\delta(\mathcal{P})^2>}}$	0.97	0.97	0.95

Table 6.1: *Results of the momentum-scaling procedure and the Nosé-Hoover thermostat at $T^* = 1.0$, and a microcanonical simulation at $E/N = -2.846$. All simulations were preformed at $\rho^* = 0.835$ for $2^{18} = 262\,144$ time steps, using 500 particles.*
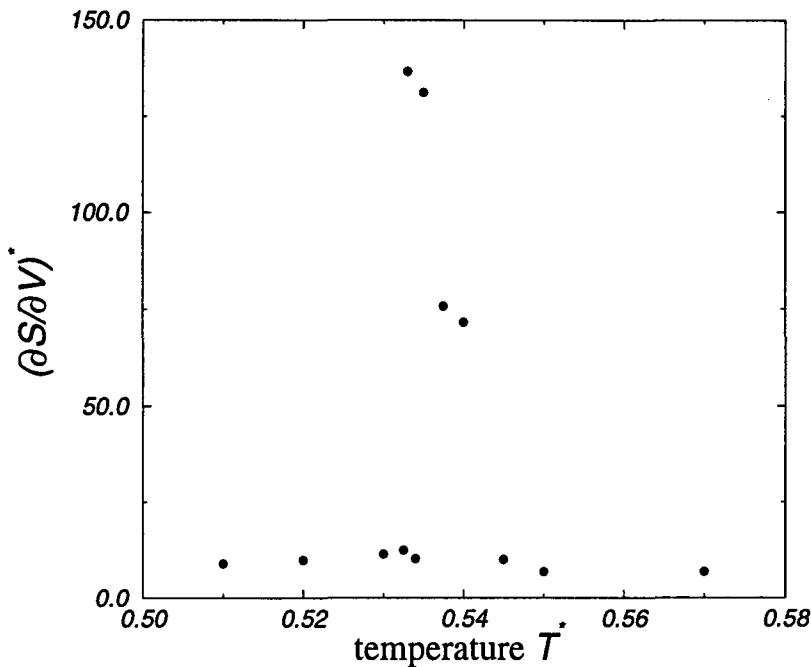
Figure 6.7: *Derivative of entropy with respect to volume.*

6.5   A short story about melting

In this section we discuss the calculation of a fluctuation corresponding to a thermodynamic derivative. An illustration is given of the Maxwell relation equation 4.15. As an example we will consider a transition that is very common in MD simulations, namely the melting transition. After all, the simulation of a liquid starts out from an overexpanded solid configuration, namely the Bravais lattice on which we placed the particles. This overexpansion, corresponding to a negative pressure, generally will force the system to melt. However, in MD simulations solid microclusters have to be superheated before they melt [31]. This suggests a kinetic barrier to melting.

We started our simulations at a relatively low temperature $T^* = 0.51$. The initial overexpanded solid did not melt at this temperature, not even after raising the temperature to 0.5325 (following the system at each temperature for approximately 250 000 time steps). At $T^* = 0.533$ the solid melted, but at $T^* = 0.534$ again it did not melt. Raising the temperature even more, forced the system to melt for each simulation we performed.

At each temperature we calculated the derivative of entropy with respect to volume, using equation 4.14. The result is shown in figure 6.7. By the Maxwell relation equation 4.15, this quantity is equal to the thermal pressure coefficient. Thus, in principal, the pressure can be obtained from these data by integration with respect to temperature. The resulting curve, together with the directly measured pressure, is shown in figure 6.8 as the solid line. The slope of the curve has the right value both for the low as the high temperatures. Only the size of the step is not in agreement with the pressure data. This is not remarkable, since the exact shape and height of the peak in 6.7 cannot be determined from the data. First of all we do not have enough data points and secondly the error bars are relatively large, varying from 30% at the top of the peak to 1% away from the peak. By applying the simple trapezium rule, it is assumed
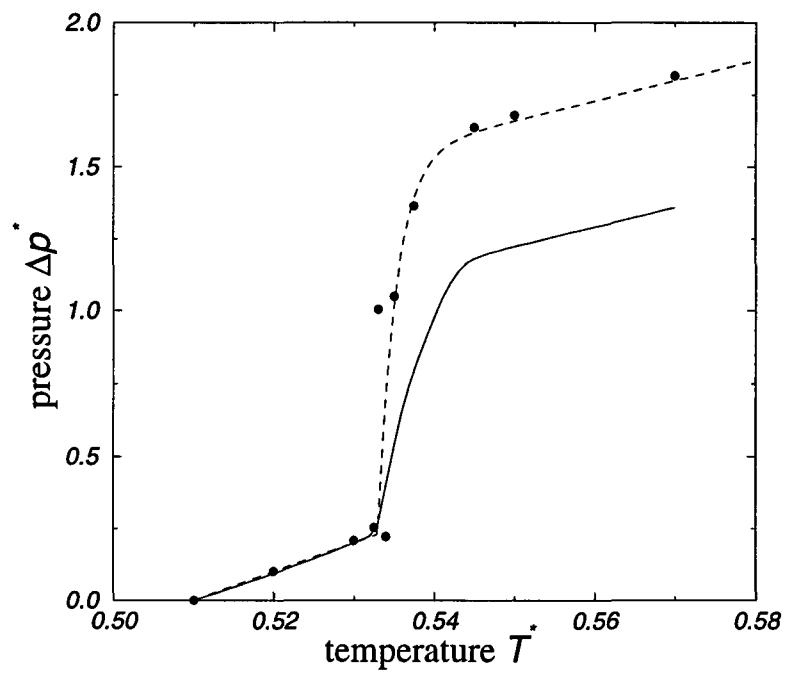
Figure 6.8: *The points are the directly measured pressure differences with the pressure $p_0 = -1.60$ at $T^* = 0.51$. The solid curve is obtained by integration, whereas the dashed curve is fitted to the data.*
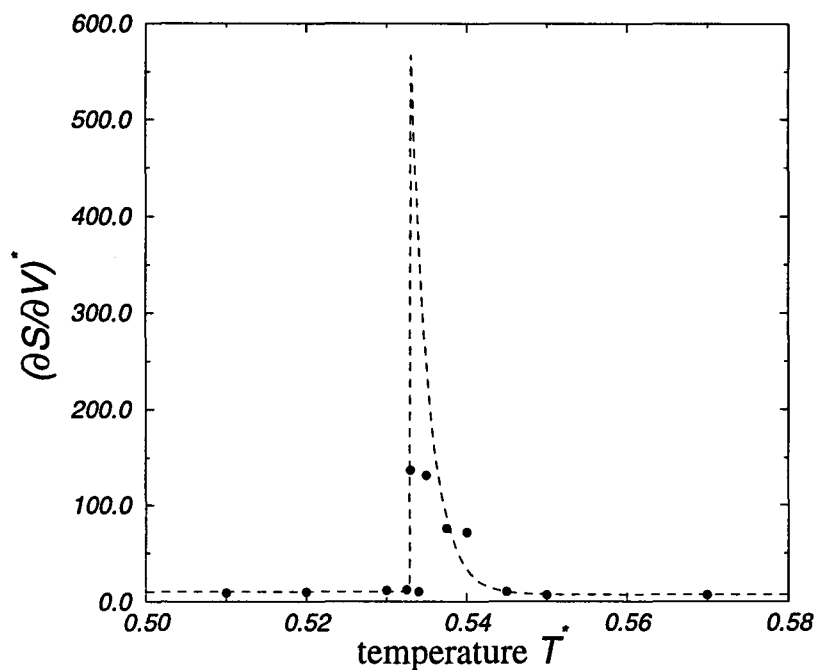
Figure 6.9: *Derivative of entropy with respect to volume. The dashed curve is obtained from differentiation of the fitted pressure curve.*

that the data are connected by straight lines. In this way a sharply peaked function can never be integrated properly, if the width of the peak and the integration step are of the same order.

We also followed another approach by fitting a function to the pressure data. Both the low and high temperature parts were taken as linear functions of slope 10 and 7, respectively. For the steeply rising part, we took the exponential form $A(1 - \exp[-a(T^* - T_c^*)])$, starting at $T_c^* = 0.533$ and fitted a and the amplitude A. The resulting curve with $a = 440$ and $A = 1.2$ is shown as the dashed line in 6.8. Differentiating this curve, a comparison can be made with the data obtained from the fluctuation formula (see figure 6.9). This concludes the technical sections and we are now in a position to start our discussion of the simulation of interfaces.

Chapter 7

The oil-water interface

7.1 Simulation set-up

In this chapter we will investigate a flat interface between two immiscible liquids, e.g. oil and water. For simplicity we will refer to the two liquids by oil and water, although the model is not that specific. Both liquids will be modelled as Lennard-Jones liquids. Interactions between an oil particle and a water particle are modelled as purely repulsive. For this repulsive potential the Lennard-Jones potential is shifted at its minimum in such a way that the potential is continuous in its second derivative, analogously to equation 6.3. As already stated, the reason for this is that the Gibbs elasticity involves second derivatives of the potential with respect to interparticle distances.

The pure oil-water system consists of $N/2$ oil and $N/2$ water particles. For the smallest simulation $N/2$ was taken $4M^3 = 500$ particles with $M = 5$. Two interfaces are made by putting half of the oil particles on top of the water particles and the other half underneath (see figure 7.1). Also simulations were performed on systems twice and four times as large in the direction perpendicular to the plane of the interfaces (the z-direction), thus having a total number of particles equal to 2000 and 4000 respectively. Always the average density of the system was set to $\rho^* = 0.835$ and the temperature to $T^* = 1.0$. The box length of the system in the plane of the interfaces is then $M (4/\rho)^{1/3} \sigma = 8.43\sigma$, corresponding to a total interfacial area of $142.1\sigma^2$.

7.2 Surface tension and system size

We measured the surface tension as a function of the system size in the z-direction. It was found that the surface tension does depend on the system size, at least for the small systems that we investigated. The surface tension without surfactants γ_0 was found to be 1.76 for $N = 1000$, 1.67 for $N = 2000$ and 1.56 for $N = 4000$ with a standard error of 0.04. This dependence can be explained from the behaviour of the particle density.

Density profiles in the z-direction are shown in figures 7.2, 7.3 and 7.4, corresponding to system sizes $N = 1000$, 2000 and 4000 respectively. These figures show that the smaller the system, the more the bulk density deviates from the average value $\rho^* = 0.835$. The repulsion across the interfaces forces the particles to move away from the interfaces into the bulk phases, thereby increasing the bulk density. For large systems, this is a negligible effect. Our systems, however, do feel this effect. Now a valid question is, whether our systems are too small to obtain quantitative results. The answer is no. Each system gives quantitative results for the bulk density which it corresponds to.[1] The smaller the system, the larger the bulk density and therefore the

---

[1] Of course, this is not true for sytems where finite-size effects are dominant.
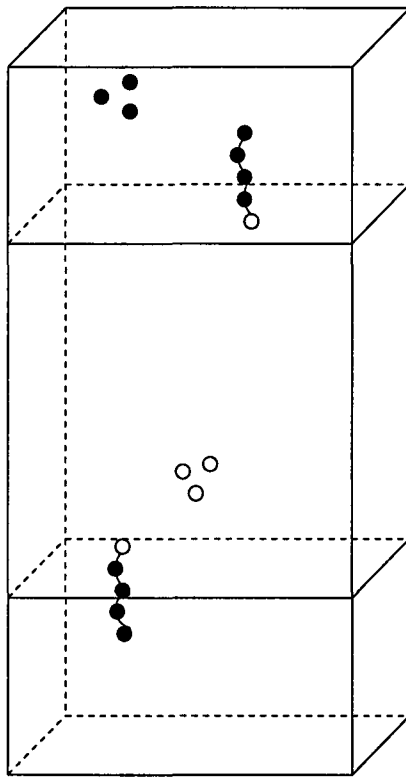
Figure 7.1: *Set-up of the simulation. Of all oil and water particles only a few are shown as black and white circles.*
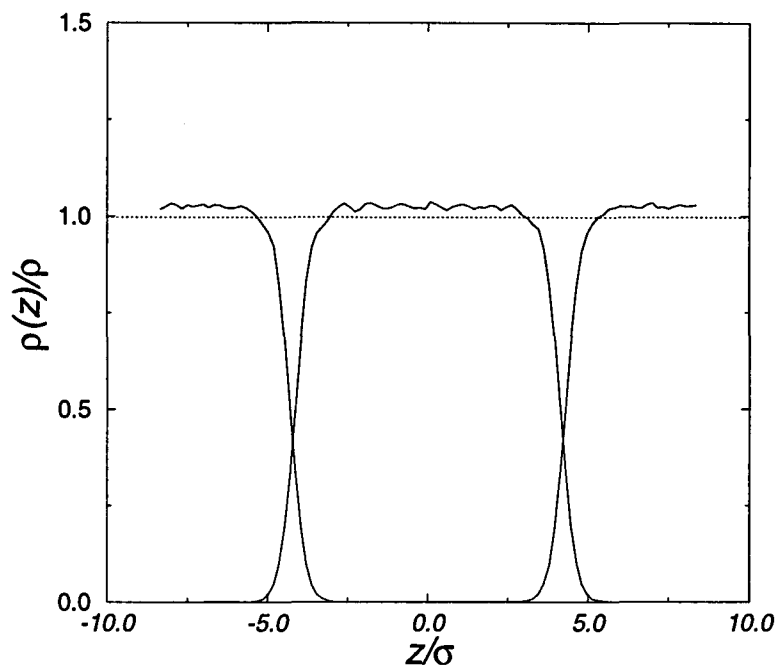
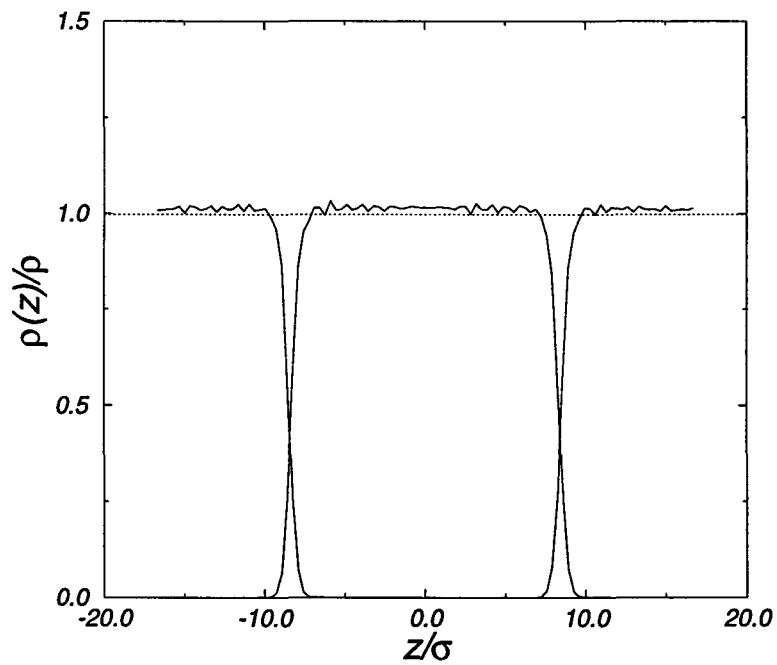Figure 7.2: *Density profile for a system of 500 oil and 500 water particles.*

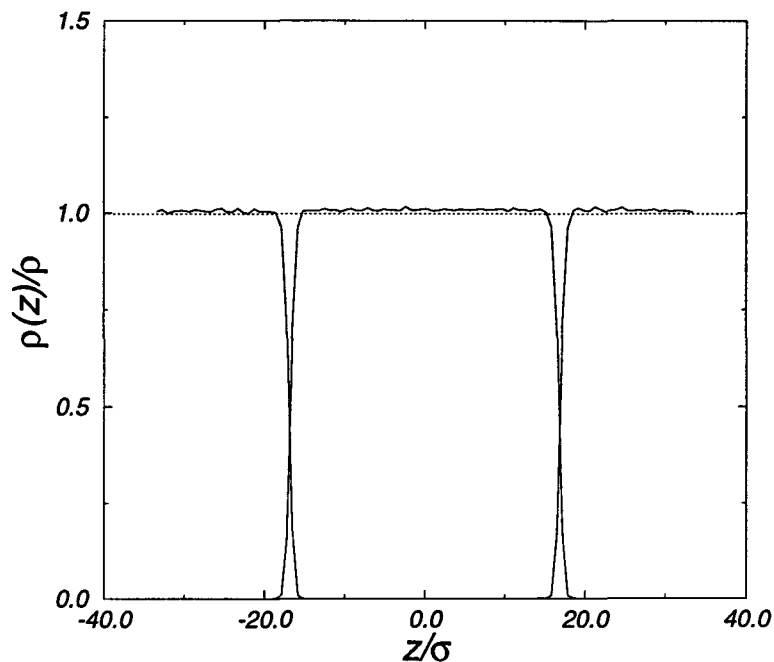Figure 7.3: *Density profile for a system of 1000 oil and 1000 water particles.*

Figure 7.4: *Density profile for a system of 2000 oil and 2000 water particles.*

larger the surface tension. Comparison of simulations at different system sizes gives information on the dependence of the surface tension on the bulk density.

7.3 Elasticity and surfactant concentration

Surfactants are modelled as consisting of a water-like head and a tail of oil-like particles [29]. We always used tails consisting of 4 oil-like particles. A water-like (oil-like) particle behaves completely as a water (oil) particle, except for the interaction with its neighbours within the molecule. Within the molecule, neigbours are held at a fixed separation a by a potential of the form

$$\widetilde{u}\left(\tfrac{1}{2}r^2\right) = \frac{K}{2a^2}\left(\frac{r^2}{2} - \frac{a^2}{2}\right)^2, \tag{7.1}$$

which for $r \approx a$ reduces to the harmonic potential $K\left(r - a\right)^2/2$. Potential 7.1 is preferred since it avoids the square root evaluation. The equilibrium bond length was chosen $a = \sigma$, whereas the bond strength K was chosen such as to minimize the fluctuations in the actual bond lengths. For large K problems can arise with the (finite time step) integration algorithm, since small displacements from equilibrium give rise to large forces. On the other hand, for small K the bonds are too weak to keep the neighbour distances constant. By trial and error the optimal bond strength can be found. A detailed treatment of inluding other intramolecular interactions as bending and torsion potentials, is given in [32].

The surfactants are added to the oil-water system at the interfaces (see figure 7.1). We always added an even number of surfactant molecules, so that they could be equally divided over the two interfaces. The head of a surfactant was placed in the layer of $2M^2 = 50$ lattice positions closest
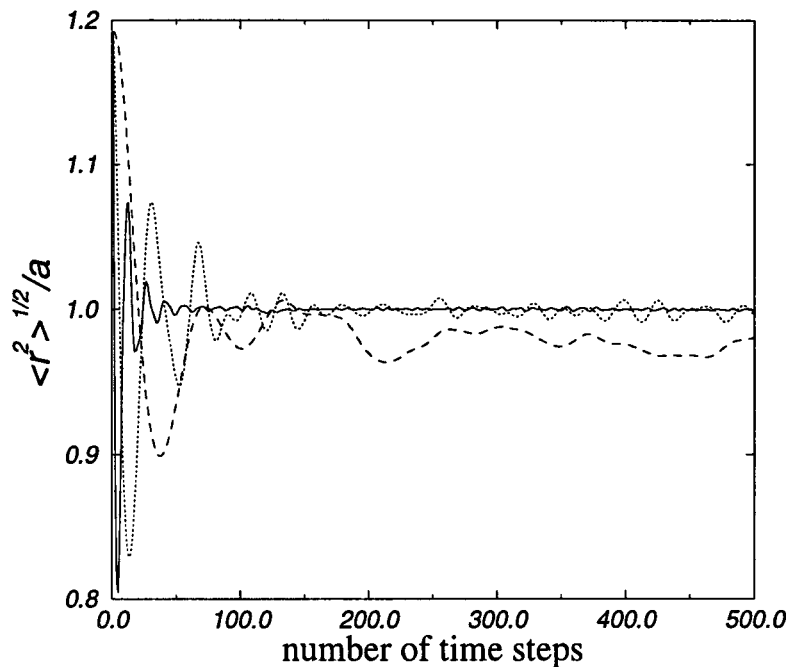
Figure 7.5: *Bond length averaged over 120 bonds (30 surfactants with 4 tail particles); the bond strength is increased by a factor 10 going from the dashed line to the dotted line and from the dotted line to the solid line; if the bond strength is further increased by a factor 10, the average bond length explodes after a few time steps.*

to the interface. Thereby a water particle is replaced by the head of the surfactant. The positions within this layer are chosen at random (of course with the limitation that two head particles may not occupy the same lattice point). The tail of the surfactant is grown from the head into the oil phase. Again the tail particles are placed on lattice positions, thereby replacing oil particles (see figure 7.9). By this construction the initial neighbour distances are $2^{-1/2}(4/\rho^*)^{1/3}\sigma \approx 1.2\sigma$. Equilibration to the equilibrium distance $a = \sigma$ is reached after a few hundred time steps for a reasonable choice of K (see figure 7.5).

Simulations were performed on the system with $N = 2000$ for various amounts of surfactants. From these simulations the surface tension and Gibbs elasticity were calculated. The results are shown in figures 7.6 and 7.7. Without surfactant molecules, the surface tension was found to be $\gamma_0^* = 1.67 \pm 0.04$ or $\gamma_0 = 21.1$ mN/m, using the argon value $\sigma^2/\epsilon = 78.9$ m/N. At zero surfactant concentration the Gibbs elasticity is practically zero, as expected for an interface of two immiscible liquids.

Gradually the surfactant concentration was increased up to a total number of 50 surfactants, corresponding to a concentration of $5\ 10^{-10}$ mol/cm^2 for liquid argon. Addition of surfactants lowers the surface tension monotonously. The Gibbs elasticity does not show a monotonous behaviour. It increases from zero and possibly shows a maximum.

According to Lucassen [4] this maximum should be present. The increase at low concentration is due to the increased surface excess. This is defined as the amount of surfactant per unit area in excess of the amount that would be present, if the surfactant would not have any preference to absorb onto the surface. The decrease at higher concentration is related to the growing
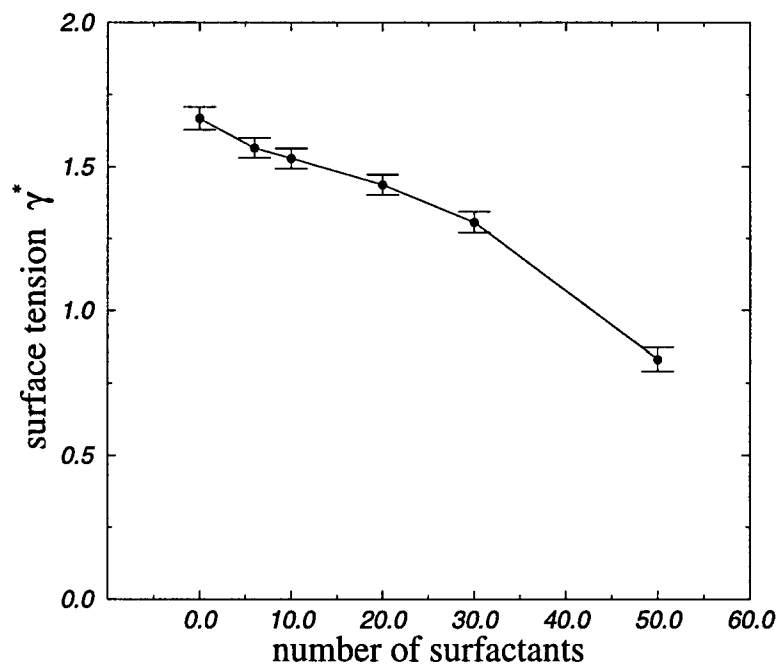
Figure 7.6: *The dependence of surface tension on the total number of surfactants added to the interfaces. The total area of the two interfaces is $142.1\sigma^2$.*
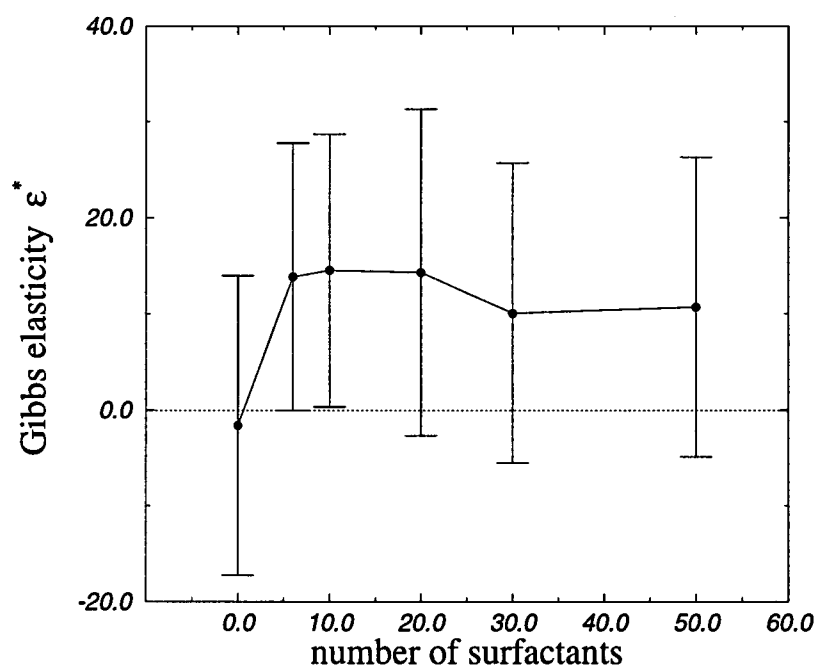
Figure 7.7: *The dependence of the Gibbs elasticity (per interface) on the total number of surfactants added to the interfaces.*

number of surfactants	$A\beta \left\langle (\delta (\partial \mathcal{U}/\partial A))^2 \right\rangle$	$A \left\langle \partial^2 \mathcal{U}/\partial A^2 \right\rangle$	ε
0	$1290.6\,(1 \pm 0.012)$	$1289.0\,(1 \pm 5\,10^{-4})$	-1.6 ± 15.6
6	$1318.3\,(1 \pm 0.011)$	$1332.2\,(1 \pm 5\,10^{-4})$	13.9 ± 13.9
10	$1349.7\,(1 \pm 0.011)$	$1364.2\,(1 \pm 5\,10^{-4})$	14.5 ± 14.2
20	$1425.7\,(1 \pm 0.012)$	$1440.1\,(1 \pm 5\,10^{-4})$	14.3 ± 17.0
30	$1508.8\,(1 \pm 0.010)$	$1518.9\,(1 \pm 5\,10^{-4})$	10.1 ± 15.6
50	$1679.1\,(1 \pm 0.009)$	$1689.8\,(1 \pm 5\,10^{-4})$	10.7 ± 15.6

Table 7.1: *Contributions to the elasticity.*

importance of the diffusional interchange of surfactant between the interfaces and the bulk phases, which, as it were, short-circuits the surface tension changes. From our simulations, we cannot decide whether this is the reason for the behaviour of the elasticity. After 250 000 time steps, we observed only 1 surfactant molecule in the oil bulk phase up to a total number of 20 surfactants. For 30 and 50 surfactants there were 3 and 5 surfactants in the oil phase, respectively. We did not observe the formation of micelles.

Note the size of the error bars in the elasticity. This is due to an almost complete cancellation of the two terms in equation 4.19 (see table 7.3). The fluctuation term, having a relative error of 1%, determines the error in the elasticity. The error bars shown are calculated using the jackknife technique described in section 5.3. We also calculated errors by dividing the simulation in 5 blocks of 50 000 time steps each (batching method). The resulting errors are in agreement with the results of the jackknife method.

We repeated the simulations described above with a different interaction between a head particle and a water particle. This interaction was increased by a factor 4, resulting in a stronger attraction (at distances larger than $2^{1/6}\sigma$). Again we varied the number of surfactants and measured the surface tension and Gibbs elasticity. As expected, the surface tension shows a stronger dependence on the number of surfactants added to the surface (see figure 7.8). The Gibbs elasticity was found to be practically zero for all concentrations. Tentatively, one could argue that this is a result of an effective repulsion between the head particles, since a head particle prefers to be surrounded by water particles.

7.4 Film thickness

In the previous section we considered a system consisting of $N/2$ oil and $N/2$ water particles, of which a certain number were replaced by surfactant particles. The thickness of the water layer in the direction perpendicular to the interfaces was globally half the box length in this direction. In this section we will decrease this thickness h by replacing a certain amount of water particles by oil particles. The surfactants are still added at the interfaces (which are now closer together) by replacing oil and water particles.

It turns out that there is a critical thickness, below which it is favourable for the water particles to form a sphere instead of a flat film. This critical thickness is easily estimated on the basis of the following macroscopic considerations. Suppose the free energy is proportional to area by the same factor for both the sphere and the film. Then the most favourable shape is that which has the lowest area. Comparison of both expressions for the area $4\pi R^2$ and $2A$ respectively, and the demand of volume conservation, i.e. $4\pi R^3/3 = hA$, gives the critical film thickness

$$h_c = \left(\frac{2A}{9\pi}\right)^{1/2} \approx 0.266 A^{1/2}. \tag{7.2}$$

To test this criterium, we performed simulations with a total number of particles $N = 1000$.
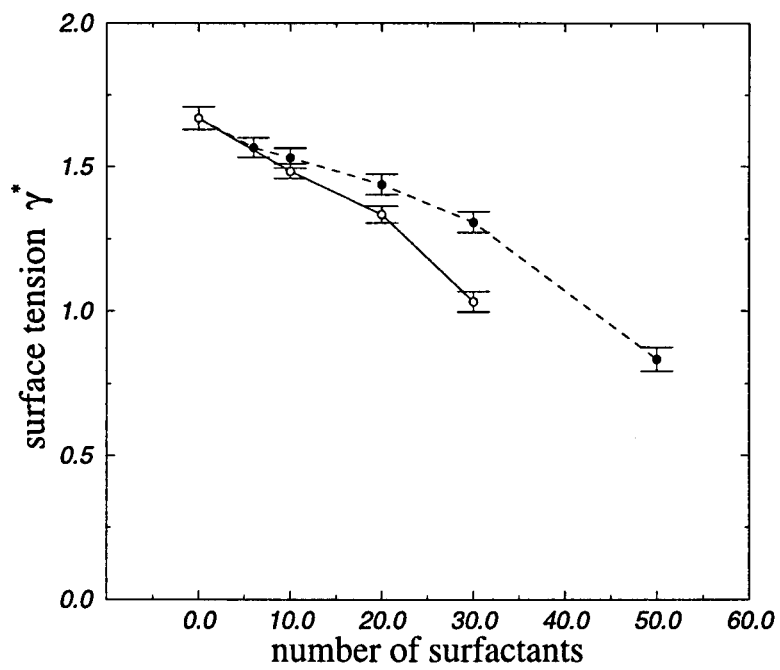
Figure 7.8: *Surface tension as a function of the total number of surfactants. The open circles correspond to an energy parameter 4ϵ for the interaction between a head particle and a water particle, instead of ϵ (filled circles).*

We varied the number of water particles (before addition of surfactants) from 500 to 100 in steps of 100. Furthermore, 30 surfactants were added to the system, all consisting of 5 particles of which 1 head particle. It was observed that a break-up of the film into a sphere only occured when the number of water particles was reduced to 100, corresponding to a film thickness $h = 0.2A^{1/2}$. Therefore, the critical film thickness is expected between $0.2A^{1/2}$ and $0.4A^{1/2}$, in agreement with equation 7.2. Since all our calculations (e.g. of surface tension) were set up for systems with a planar symmetry, we only give qualitative information on this system. The time evolution of the system is depicted in figures 7.9 to 7.12, where the configuration of the surfactant and water molecules is shown.

Simulations on systems of 200 and more water particles did not show this break-up phenomenon. They kept their flat interfaces even after 500000 time steps. The surface tension was only weakly dependent on the film thickness in this range (see figure 7.13). We measured γ^* to be equal to 1.28, 1.31, 1.30 and 1.36 for film thicknesses h equal to $A^{1/2}$, $0.8A^{1/2}$, $0.6A^{1/2}$ and $0.4A^{1/2}$ respectively.

We were not able to perform a study of film elasticity on film thickness. This dependence is governed by diffusional interchange of surfactants between the solution and the surfaces. In our simulation set-up we were not able to study these diffusion processes, since the time and length scales involved are too large. Realistic film thicknesses are of the order of 1 μm, giving a diffusion time of the order of 1 ms (diffusion coefficient D of the order of 10^{-6} cm^2/s). In our simulations film thicknesses are of the order of a few nanometers, whereas the maximum time that can be simulated is of the order of 10 ns (corresponding to 10^6 time steps for argon).
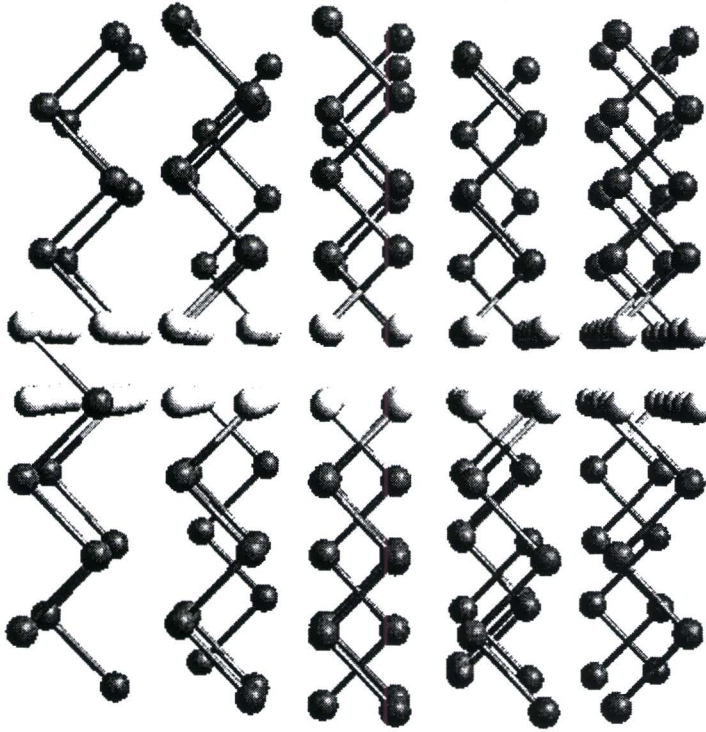
Figure 7.9: *Configuration of the system at the beginning of the simulation. The head particles are represented by white spheres connected to a tail of gray spheres. Water particles are represented by single white spheres. Oil particles are not shown, but occupy the remaining lattice points. The bonds are of a length $\approx 1.2\sigma$. Note that the sphere radius is smaller than the Lennard-Jones parameter σ.*
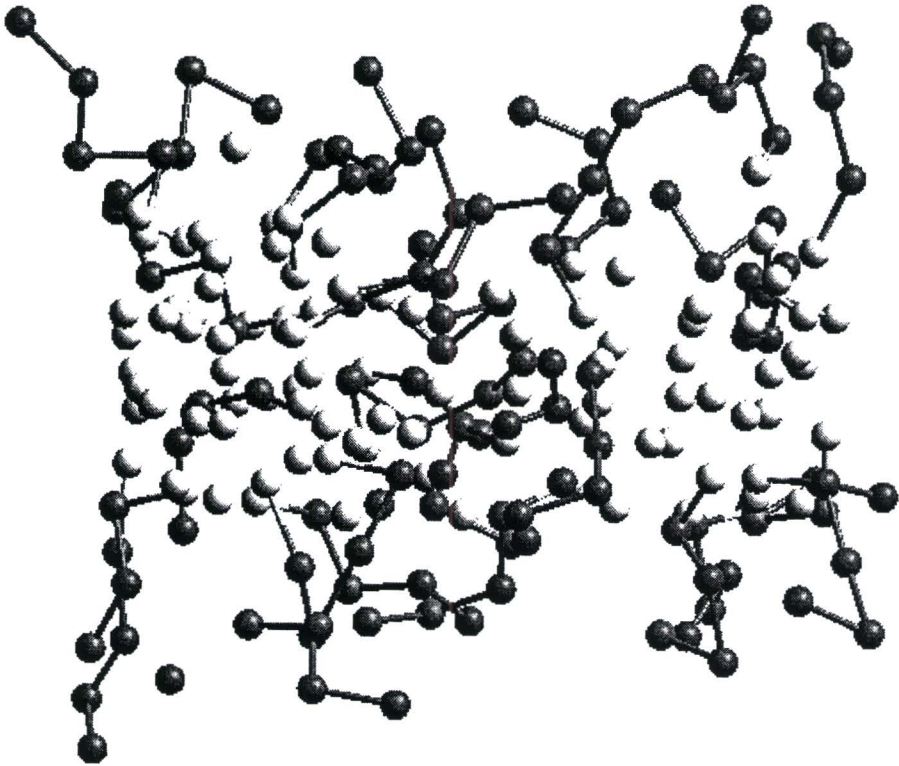
Figure 7.10: *Configuration after 5000 time steps. The bond lengths have equilibrated to their equilibrium value σ.*
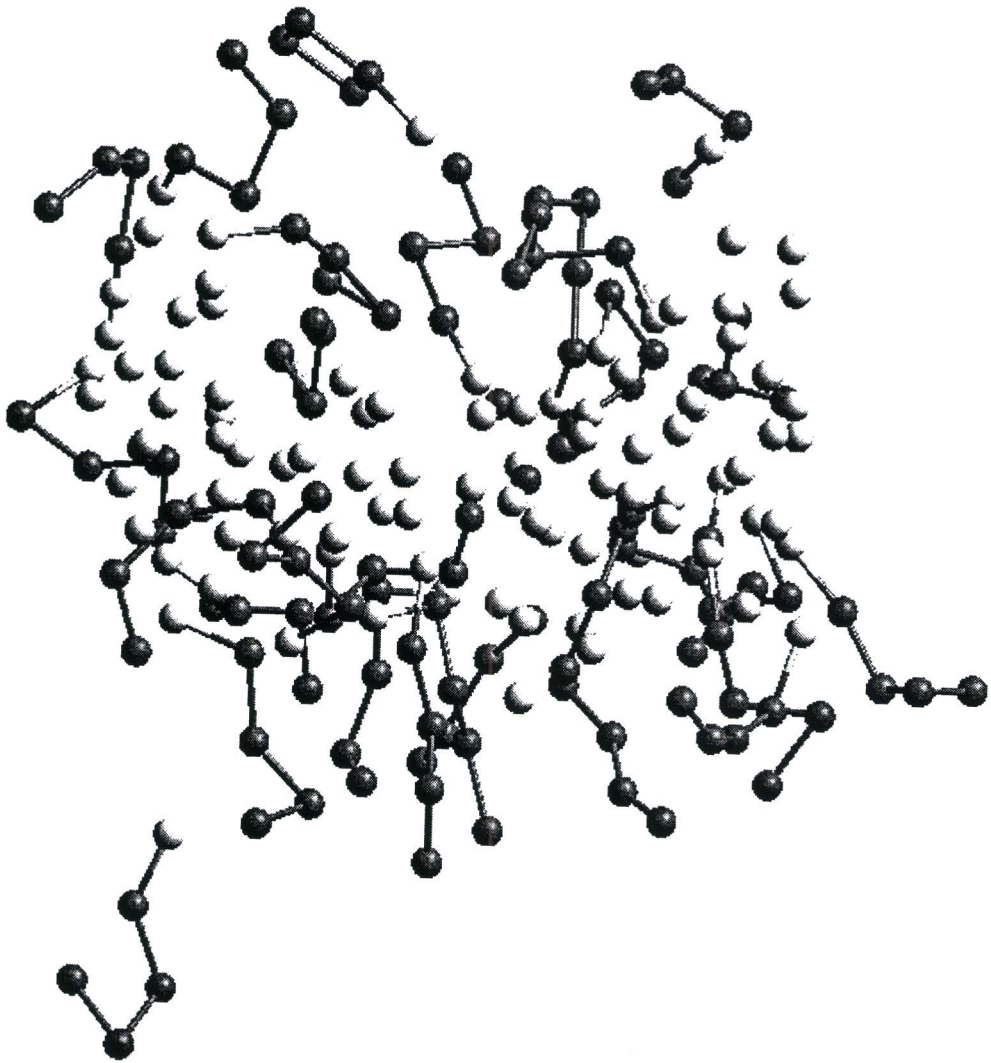
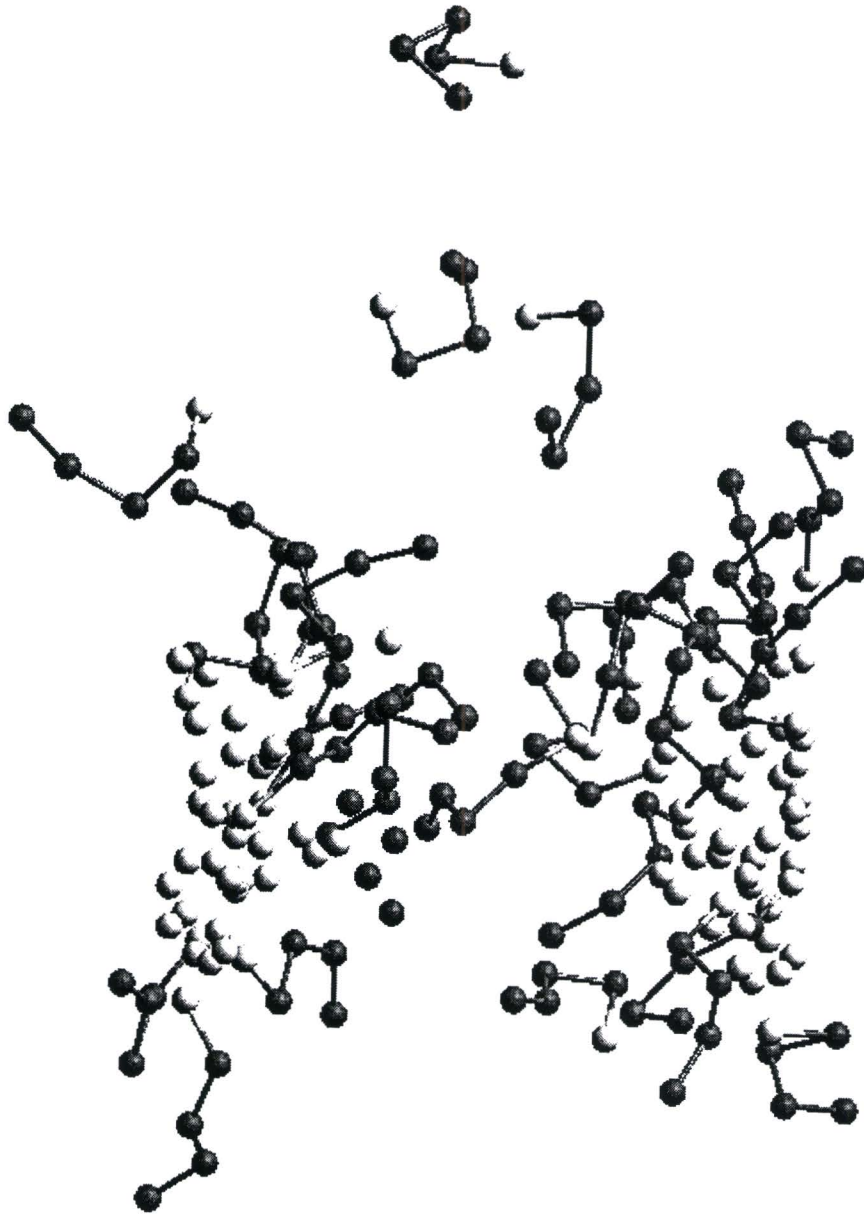Figure 7.11: *Configuration after approximately* 250 000 *time steps.*

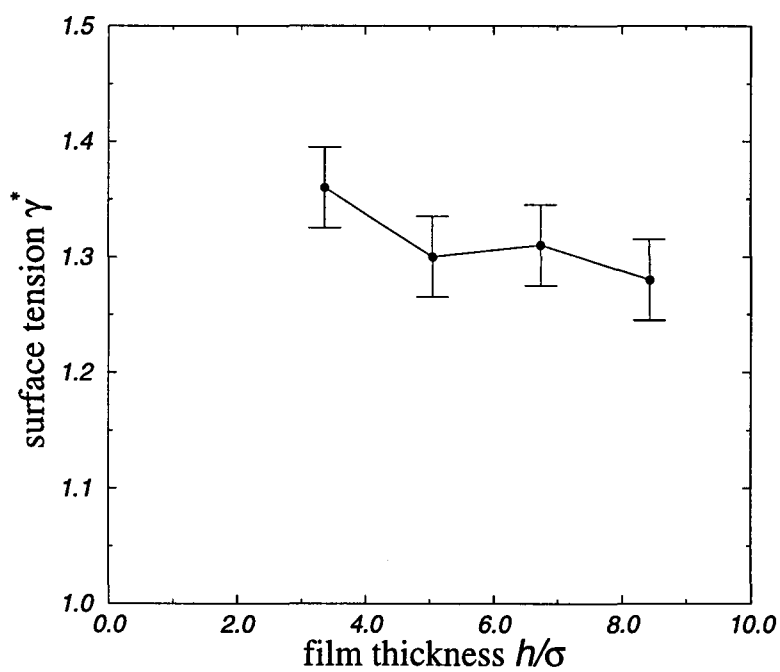Figure 7.12: *Configuration after approximately* 500 000 *time steps.*

Figure 7.13: *The dependence of the surface tension on the thickness of the water layer for a system of 1000 particles in which 30 surfactants are present.*

Chapter 8

Conclusion

In this thesis a study of the stability of liquid films and foams was performed. The Gibbs elasticity of interfaces was studied by simulation. To this end a Molecular Dynamics program has been developed. A comparison was made between two methods of constant-temperature Molecular Dynamics, namely momentum scaling and Nosé-Hoover thermostatting, and conventional constant-energy Molecular Dynamics. The motive is that, since the Gibbs elasticity is a fluctuation, it is expected to be strongly dependent on the quality of the thermostat.

An illustration of thermodynamic integration was given by an artificial melting transition. The thermal pressure coefficient was obtained both indirectly from the measured pressure and directly from the measured volume dependence of the entropy, involving a fluctuation.

The calculation of any quantity by simulation is subject to statistical uncertainties. Although error estimation for fluctuations is not trivial, we were able to estimate the uncertainty in the calculated Gibbs elasticities. Due to an almost complete cancellation of the two terms contributing to the Gibbs elasticity, the relative uncertainty was found to be of the order one. Here it concerned simulations taking approximately two days on the IBM Scalable Power 2, to obtain the elasticity at a given concentration. Longer simulation are needed to increase the accuracy of the resulting elasticities.

Despite these uncertainties, the calculated dependence of the Gibbs elasticity on the concentration of surfactants followed the trends of the expected behaviour, as discussed by [4]. We also observed a stronger concentration dependence of the surface tension, after increasing the attraction between the water and the head of the surfactant.

The break-up of a thin and flat film into a sphere was observed at a thickness below the predicted critical thickness. In the sphere, consisting of water, the surfactants pointed their heads inward and their tails towards the oil phase. As expected, films thicker than the critical thickness did not break up. For these films, we observed a small dependence of the surface tension on film thickness.

Bibliography

[1] J.W. Gibbs, *The collected works of J. Willard Gibbs, volume 1: thermodynamics*, Yale University Press (1948).

[2] A. Prins, C. Arcuri and M. van den Tempel, J. Colloid Interface Sci. **24**, 84 (1967).

[3] J. Lucassen and D. Giles, J. Chem. Soc. Faraday I **71**, 217 (1975).

[4] J. Lucassen, in: *Anionic surfactants: physical chemistry of surfactant action*, ed. E.H. Lucassen-Reynders, Dekker, New York (1981).

[5] D. Weaire and N. Rivier, Contemp. Phys. **25**, 59 (1984).

[6] J.A. Glazier and D. Weaire, J. Phys.: Condens. Matter **4**, 1867 (1992).

[7] G. Verbist and D. Weaire, Europhys. Lett. **26**, 631 (1994).

[8] J.P. Hansen and I.R. McDonald, *Theory of simple liquids*, Academic Press (1986).

[9] J.L. Lebowitz, J.K. Percus and L. Verlet, Phys. Rev. **153**, 250 (1967).

[10] J.R. Ray and H.W. Graben, Mol. Phys. **43**, 1293 (1981).

[11] E.M. Pearson, T. Halicioglu and W.A. Tiller, Phys. Rev. A **32**, 3030 (1985).

[12] N. Metropolis, A.W. Rosenbluth, M.N. Rosenbluth, A.H. Teller and E. Teller, J. Chem. Phys. **21**, 1087 (1953).

[13] A.Z. Panagiotopoulos, Mol. Phys. **61**, 813 (1987).

[14] M.P. Allen and D.J. Tildesley, *Computer simulation of liquids*, Oxford University Press (1989).

[15] S. Nosé, J. Chem. Phys. **81**, 511 (1984).

[16] H.C. Andersen, J. Chem. Phys. **72**, 2384 (1980).

[17] S. Nosé, Mol. Phys. **52**, 255 (1984).

[18] W.G. Hoover, Phys. Rev. A **31**, 1695 (1985).

[19] S. Nosé, Mol. Phys. **57**, 187 (1986).

[20] S. Toxvaerd, Mol. Phys. **72**, 159 (1991).

[21] G.J. Martyna, M.L. Klein and M. Tuckerman, J. Chem. Phys. **97**, 2635 (1992).

[22] H.S. Green, Proc. Roy. Soc. (A) **189**, 103 (1947).

[23] D.A. McQuarrie, *Statistical mechanics*, Harper and Row (1976).

[24] F.P. Buff, Z. Elektrochem. **56**, 311 (1952).

[25] C.G. Gray and K.E. Gubbins, *Theory of molecular fluids, volume 1: fundamentals*, Oxford University Press (1984).

[26] H. Flyvbjerg and H.G. Petersen, J. Chem. Phys. **91**, 461 (1989).

[27] B. Efron, SIAM Review **21**, 460 (1979).

[28] M.M. Telo da Gama and K.E. Gubbins, Mol. Phys. **59**, 227 (1986).

[29] B. Smit, *Simulation of phase coexistence: from atoms to surfactants*, Ph.D. thesis, Rijksuniversiteit Utrecht (1990).

[30] S. Karaborni, N.M. van Os, K. Esselink and P.A.J. Hilbers, Langmuir **9**, 1175 (1993).

[31] D. Frenkel and J.P. McTague, Ann. Rev. Phys. Chem. **31**, 491 (1980).

[32] I. van Gerwen, *Elasticiteitsberekeningen voor schuim*, Eindhoven University of Technology (1993).

Appendix A

Pair-wise additive potentials

If the interactions are pair-wise additive and dependent on interparticle distances only, the potential energy can be written as

$$\mathcal{U} = \sum_i \sum_{j>i} u\left(\tfrac{1}{2}r_{ij}^2\right).$$

(A.1)

The radial dependence is written in terms of squared interparticle distances, since these are directly available in a simulation. In this way, we can avoid taking square roots in order to obtain the interparticle distances themselves.

For additive potentials it is convenient to introduce the virial function $\mathcal{W}$ as

$$\frac{\mathcal{W}}{V} = -\frac{\partial \mathcal{U}}{\partial V} = -\frac{1}{3V} \sum_i \sum_{j>i} r_{ij}^2 u'\left(\tfrac{1}{2}r_{ij}^2\right),$$

(A.2)

and the instantaneous surface tension Γ as

$$\Gamma = \frac{\partial \mathcal{U}}{\partial A} = \frac{1}{2A} \sum_i \sum_{j>i} \left(x_{ij}^2 + y_{ij}^2 - 2z_{ij}^2\right) u'\left(\tfrac{1}{2}r_{ij}^2\right).$$

(A.3)

This quantity has no contributions from isotropic regions. Therefore only the interfaces contribute to the surface tension.

Finally, the second derivative of the potential energy with respect to area can be written explicitly as

$$\frac{\partial \Gamma}{\partial A} = \frac{1}{(2A)^2} \sum_i \sum_{j>i} \left(\left(r_{ij}^2 - 3z_{ij}^2\right)^2 u''\left(\tfrac{1}{2}r_{ij}^2\right) + 12 z_{ij}^2 u'\left(\tfrac{1}{2}r_{ij}^2\right) \right)$$

(A.4)